**Understanding the forest structure:**

**Development of tools for identification and delineation of individual trees using LiDAR**

by

Rafael Loos
B.Sc., Universidade Federal de Viçosa, 2003

A Thesis Submitted in Partial Fulfillment
of the Requirements for the Degree of

MASTER OF SCIENCE

in the Department of Geography

# Supervisory Committee

**Understanding the forest structure:**

**Development of tools for identification and delineation of individual trees using LiDAR**

by

Rafael Loos
B.Sc., Universidade Federal de Viçosa, MG - Brazil, 2003

**Supervisory Committee**

Dr. K. O. Niemann, (Department of Geography)
**Supervisor**

Dr. T. Nelson, (Department of Geography)
**Departmental Member**

Dr. M. S. Flaherty, (Department of Geography)
**Departmental Member**

# Abstract

**Supervisory Committee**

Dr. K. O. Niemann, (Department of Geography)
**Supervisor**

Dr. T. Nelson, (Department of Geography)
**Departmental Member**

Dr. M. S. Flaherty, (Department of Geography)
**Departmental Member**

LiDAR (Light Detection and Ranging) is currently being used to extract the biophysical characteristics of forests. LiDAR can provide extensive information about tree canopies; pulses reflected back to the sensor can represent understory vegetation as well as partial tree canopies below the dominant trees. Canopy structure can yield valuable clues about the biodiversity, and processes affecting the ecology of forest stands. In addition, structural information can provide insight into other processes such as fire behaviour and the distribution of fuels. This thesis focuses in developing tools to better understand the forest structure. The tools are computer-based algorithms that use LiDAR data as input and provide output with detailed information about the different layers of vegetation in a forested area. Three main modules are used in this study: (1) treetop identification, (2) delineation of canopies for the dominant layer of vegetation, and (3) delineation of partial canopies underneath this dominant layer. The study area was located in the Greater Victoria Water District, west of Victoria, British Columbia, Canada. Nine plots were chosen to represent the study area. A complete census was conducted in the summer of 2005 to provide information about tree, diameter at breast height (DBH), and tree dominance (based on the criteria: suppressed, intermediate, co-dominant and dominant). Results show that the algorithm is able to properly identify and delineate the majority of trees in the study areas. The third module, partial canopy delineation, also presents promising results with the dataset used. Newer LiDAR systems, with higher number of returns, will definitely provide better datasets with more information of the different layers within the forest, increasing the identification and delineation of these partial trees. Need of new field data is a must for future work and for further tests with the algorithm.

# Table of Contents

Supervisory Committee ..... ii
Abstract ..... iii
Table of Contents ..... iv
List of Tables ..... vi
List of Figures ..... vii
Acknowledgements ..... ix
Chapter 1: Introduction ..... 1
Chapter 2: Objectives and research questions ..... 4
Chapter 3: The LiDAR sensor ..... 5
3.1 – Remotely-sensed data and individual tree identification ..... 8
3.2 – Computer algorithms for LiDAR data ..... 11
3.3 – LiDAR data and individual tree identification ..... 13
Chapter 4: Study Area ..... 16
4.1 - General Description ..... 16
4.2 - Rithet Creek Valley ..... 17
4.2.1 - Rithet Creek ..... 17
4.2.2 - Dominant Tree Species ..... 18
4.3 - Douglas-fir and a digital form ..... 18
Chapter 5: Methods ..... 20
5.1 - LiDAR data ..... 20
5.2 – Data collection ..... 20
5.2 – Processing the LiDAR data for treetop identification and canopy delineation ..... 26
5.2.1 - Extracting ground and vegetation points ..... 26
5.2.2 - Gridding the ground ..... 27
5.2.3 - Vegetation file ..... 29
5.2.4 - Subtracting the DEM from the vegetation points ..... 30
5.2.5 - Treetops detection and canopy delineation algorithm ..... 32
5.3 – Validation between field and algorithm coordinates ..... 39
5.4 - Partial crown delineation ..... 45
Chapter 6: Results ..... 49
6.1 – Individual treetop identification ..... 49
6.2 – Crown delineation ..... 54
6.3 - Partial crown delineation ..... 59
6.3.1 – Intermediate-growth plots ..... 59
6.3.2 – Old-growth plots ..... 67
Chapter 7: Discussion ..... 76
7.1 – Tree crowns ..... 76
7.2 – Treetop identification ..... 77
7.3 – Matching surveyed and identified treetops ..... 78
7.4 – Crown delineation ..... 79
7.4.1 – Young-growth plots ..... 79
7.4.2 – Intermediate-growth plots ..... 80

7.4.3 – Old-growth plots ..... 81
7.5 – Partial crowns identification ..... 82
Chapter 8: Conclusion ..... 84
8.1 – Conclusions ..... 84
8.2 – Future work ..... 85
Bibliography ..... 86
Appendix A – Study plots with tree locations ..... 92

# List of Tables

Table 1 - Details about the nine surveyed plots. ..... 22
Table 2 - Plots statistics. ..... 24
Table 3 - Calculation of X and Y coordinates for every iteration. ..... 35
Table 4 - Height thresholds used in matching algorithm. ..... 43
Table 5 - Summary of all surveyed plots. ..... 54
Table 6 - Summary of number of partial-canopies identified. Column “Surveyed” represents the “intermediate” and “suppressed” trees surveyed in the field, while column “Identified” represents the number of trees identified by the algorithm based on the LiDAR points available below the TSCL threshold. ..... 75

# List of Figures

Figure 1 - Measurement principle of LASER scanning over forest areas. ..... 5
Figure 2 - Location of the study area. Individual watersheds within the CRD water land base (red boundaries). Shaded area represents the study area, Rithet Creek valley. ..... 17
Figure 3 - Projected crown area on the ground. ..... 19
Figure 4 - Photos showing in more details the distribution of trees within plots. ..... 21
Figure 5 - Tree dominance: D – dominant trees; CD – co-dominant trees; I – intermediate trees; and S – suppressed trees. ..... 23
Figure 6 - Height vs. DBH for young-growth plots. ..... 24
Figure 7 - Height vs. DBH for intermediate-growth plots. ..... 25
Figure 8 - Height vs. DBH for old-growth plots. ..... 25
Figure 9 - Flowchart displaying steps for creation of CHM. ..... 26
Figure 10 - Simple example of triangulating some LiDAR ground points. (a) shows the circumcircles being added around points. A triangle will be a valid triangle if and only if a circumcircle holds no other point of the point set. (b) shows the points connected, creating the triangles. (c) shows the method where a point is added in the set of points and new circumcircles being examined. (d) shows the new triangles formed after the newly added point. The red line represents the convex hull that contains all the ground points. ..... 28
Figure 11 - DEM with resolution of 2 x 2 m after gridding process ..... 29
Figure 12 - DSM created with vegetation points extracted from the LiDAR data. ..... 30
Figure 13 - Subtraction procedure. (a) Birds-eye view of ground cell. (b) Side-view of LiDAR points within cell. (c) Tree heights without elevation effect. ..... 31
Figure 14 - CHM created after subtracting the DEM from the DSM. ..... 31
Figure 15 - Clockwise addition of 10 degrees for every iteration. ..... 34
Figure 16 - Example of the first iteration facing the north direction. The code searches for the closest heights for every 0.5 m mark. ..... 36
Figure 17 - Showing the two situations the algorithm might handle; edges between two trees and edges between tree and ground. ..... 37
Figure 18 - Treetop identification and canopy delineation algorithm flowchart. ..... 38
Figure 19 - Matching treetops with field and algorithm data. Buffer size for the extreme case that might occur in the field. ..... 41
Figure 20 - Height threshold calculation ..... 42
Figure 21 - Treetop validation flowchart. ..... 44
Figure 22 - Comparison between Height to Living Crown (HLC) and the top of suppressed canopy level (TSCL). ..... 46
Figure 23 – Simulated percentile and derivative curves showing the location of the abrupt change in curvature. ..... 47
Figure 24 - Partial canopy delineation flowchart. ..... 48
Figure 25 - LiDAR CHM data as background, treetops represented as blue dots and plot boundary as red polyline. Red squares represent tree locations matched with field data. 50
Figure 26 - Results of identified and surveyed trees per plot. ..... 54

Figure 27 - LiDAR CHM data as background, treetops represented as blue dots and plot boundary as blue polyline. Red polygons represent delineated crowns. ..... 55
Figure 28 - Results of average radii of crowns measured in the field and outlined by the algorithm. ..... 58
**Figure 29 - Chart containing percentile and derivative curves for intermediate-growth plots. Red line indicates TSCL in metres.** ..... 61
Figure 30 - Top figure shows a plan-view of plot 1, and bottom figure a vertical profile for the same plot. Green dots represent dominant trees; brown dots represent trees underneath dominant layer. ..... 63
Figure 31 - Top figure shows a plan-view of plot 4, and bottom figure a vertical profile for the same plot. Green dots represent dominant trees; brown dots represent trees underneath dominant layer. ..... 64
Figure 32 - Top figure shows a plan-view of plot 7, and bottom figure a vertical profile for the same plot. Green dots represent dominant trees; brown dots represent trees underneath dominant layer. ..... 65
Figure 33 - Plan-view of intermediate-growth plots showing LiDAR points below TSCL. ..... 67
Figure 34 - Chart containing percentile and derivative curves for old-growth plots. Red line indicates TSCL in metres. ..... 69
Figure 35 - Top figure shows a plan-view of plot 2, and bottom figure a vertical profile for the same plot. Green dots represent dominant trees; brown dots represent trees underneath dominant layer. ..... 71
Figure 36 - Top figure shows a plan-view of plot 5, and bottom figure a vertical profile for the same plot. Green dots represent dominant trees; brown dots represent trees underneath dominant layer. ..... 72
Figure 37 - Top figure shows a plan-view of plot 8, and bottom figure a vertical profile for the same plot. Green dots represent dominant trees; brown dots represent trees underneath dominant layer. ..... 73
Figure 38 - Plan-view of old-growth plots showing LiDAR points below TSCL. ..... 74
Figure 39 - Uniform conifer tree shape on the left and tree with broken top and multiple tops on the right. ..... 77

# Acknowledgements

After all these years battling with this manuscript, this is the most difficult section to write. It is difficult not because I don't know who to thank, but because it is not easy how to find the best words to thank them for all their time and patience with me.

First, I have to thank Olaf for giving the opportunity to an Agronomic Engineer, used to take care of plants, to land in a different country and find a place to work and to pursue a new future. I thank him for all the knowledge passed on to me, especially because I had no clue what a LiDAR system was.

My brother Eduardo... I think I will not be able to express all my gratitude in words ... I thank you for all the help with my English grammar. Thank you for being really patient with me through some stressful times ... Thank you for always being there for me ... Thank you for being my brother.

Another person that I could not leave out of this section is one crazy Italian that I met along the master's crooked road. Fabio, thank you for being my friend, for sticking with me through some crazy fieldwork, and for teaching me all about the Italian cuisine ... Someday I will learn how to make proper pasta.

My special thanks to Jaden and Francois for helping me with the data collection and for making the forest a pleasant place during fieldwork.

# Chapter 1: Introduction

Forests are vital in sustaining a liveable environment for many living organisms on Earth, balancing the ecosystem by preserving and recycling usable resources such as water. Forests are constantly changing due to natural phenomena, such as the weather (wind, rain), other organisms (insects, fungi), and humans (deforestation, urbanization, pollution). To understand the health of forests one needs to assess every aspect of the forest, recognizing every factor that affects its health.

A well-structured forest will provide shelter and nutrients for organisms, and also provide a perfect environment for the development of healthy trees. Not only will other organisms benefit from that, but also humans will be able to extract better quality of primary products such as wood from this environment. With a well-planned harvesting strategy, based on the better information and knowledge about the forest structure, it is possible to reduce the amount of damage and disturbance caused to the forest health, keeping the ecosystem in balance.

It is important to be concerned about quality and health of the primary product. Canada is the leading producer and exporter of newsprint in the world. Satisfying the market with an excellent product strengthens the demand for this product. In Canada, the forest sector provides more than 294,000 direct jobs, including the paper and the wood industry. The contribution in 2007 to the Gross Domestic Product (GDP) reached close to $31 billion Canadian dollars (Natural Resources Canada, 2007). In British Columbia, with a population over 4.4 million (BCStats, 2008), the forestry sector provided more than 84,000 direct jobs and contributed more than 12 billion dollars to the GDP in 2007.

It is important to understand the forest structure in order to assess the health of the forests. With the advances in technology, the remote sensing industry is able to provide tools capable to provide a reliable and fast way of extracting information from forested areas. Airborne LiDAR (Light Detection And Ranging) is one example, being an accurate and fast-response tool for extracting three-dimensional attributes from a particular area. Its development started in the 1970's with focus on bathymetric and hydrological applications (Wehr et al., 1999). During the 1980's, with the development of more precise Global Positioning Systems (GPS), LiDAR started to gain in importance. LiDAR systems were used primarily for acquiring Digital Terrain Models (DTM) in the mid 90's (Lohr, 2003) with great potential for large-scale projects (Ackermann, 1999). Consequently, LiDAR systems are the preferred system for acquiring DTM's and Digital Surface Models (DSM's) of forested areas. These systems are characterized by the width of the LASER beam footprint and by how the return pulse is recorded. According to beam width, LiDAR systems fall into two categories: large-footprint or small-footprint; and based on recording pulses: discrete return or full-waveform (Bortolot et al., 2005). Systems presenting a small footprint and multiple discrete returns collect data on the different levels of tree canopy, understory vegetation, and bare-earth data. Discrete return systems usually present footprint size ranging from 0.2 m to 0.9 m, while full-waveform footprints vary from 8 m to 70 m (Lim et al., 2003). The disadvantage of these systems, because of the small footprint size, is the possibility of not acquiring treetops. Treetops are characterized in remote sensing data as being the brightest pixel in a raster image or the highest value in a Canopy Height Model (CHM) produced from classified LiDAR data.

The primary objective of this thesis is to develop a better understanding of the forest cover through the segmentation of tree canopies. This is possible by mapping tree locations in the study area, outlining their canopies, and differentiating higher vegetation from understory vegetation. With the development of computer algorithms to process and analyse datasets, new and improved visualization of areas that require special attention will be presented.

# Chapter 2: Objectives and research questions

The primary objective of this thesis is to develop computer algorithms to analyse and process LiDAR datasets of forested areas. These algorithms need to identify individual trees in a forest, acquire their location by recording their geographic location, and be able to delineate each individual tree canopy. To assess the accuracy of each algorithm output, field data were collected for each study plot, presenting a full census of the tree population within each plot. Also, an accuracy assessment was performed by algorithms developed for this study. Furthermore, the identification of individual trees underneath the dominant vegetated surface cover was also performed.

For this research, the questions addressed were:

1. How can individual trees, in dense managed and unmanaged forested areas, be identified from airborne LiDAR data?
2. Can individual tree canopies be delineated?
3. If so, can trees be identified and mapped underneath the dominant/co-dominant layer of vegetation?

The objectives based on the research questions are as follows:

1. To create algorithms to identify the tops of the trees from LiDAR data taking into account individual tree heights;
2. To develop procedures to delineate and extract individual canopy outlines from the LiDAR canopy height data;
3. Creation of an algorithm to identify and map total or partial trees underneath dominant trees.

# Chapter 3: The LiDAR sensor

LiDAR is an active sensor that collects height data using pulses of LASER light as a source of energy (Kraus and Pfeifer, 1998). The system records the total time that an emitted pulse takes to travel from the sensor to an object close to the surface and back to the sensor. This time is used to calculate the distance from the sensor to the object and therefore identify its altitude (Wehr and Lohr, 1999). Positional (horizontal and vertical) data are acquired at the same time by using an on-board differential GPS (dGPS), which communicates with a ground station and an Inertial Measurement Unit (IMU) (Lim et al., 2001) (Figure 1). The IMU records the roll, pitch, and yaw of the aircraft to determine its orientation, while the dGPS records the airplane's location (Wehr and Lohr, 1999).

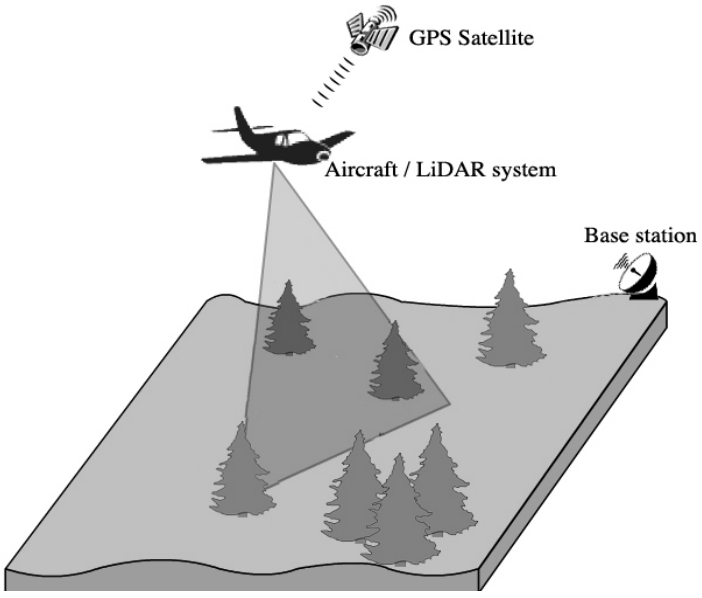


**Figure 1 - Measurement principle of LASER scanning over forest areas.**

Airborne LiDAR data can be used to derive information regarding forest biophysical characteristics, providing information on topography, tree heights, stem density, crown

dimensions, and gap structure (Popescu et al., 2002). Usually the acquisition of such data requires manual field-based procedures that are labour-intensive, time-consuming and also susceptible to subjective errors (Hopkinson et al., 2004).

To extract information while flying over forested areas, LiDAR systems like any other remote sensing instrument, need to be well-calibrated prior to data collection. One needs to be aware of the many system and vegetation-based variables, which can introduce problems to the datasets, in order to assure collecting data with excellent quality. Quality is affected by the frequency of the LiDAR system which regulates the maximum height of flight for the aircraft, and the loss in energy of the LiDAR pulse as altitude increases. Also, atmospheric noise degrades the return signal to the point where the energy falls below the detection limits of the system (Gómez, 2005).

After a quality assured data acquisition, the position and orientation values gathered by the dGPS and IMU are used to georeference the ranging measurements. LiDAR produces a 3D dataset of elevation points X (easting), Y (northing), and Z (elevation) for the ground surface and objects. Point density will vary depending on flying height, aircraft speed, field of view (FOV) and frequency of the pulses (Axelsson, 1999).

LiDAR systems, as described in the introduction chapter, fall into two categories: large-footprint or small-footprint; and based on recording pulses: discrete return or full-waveform (Bortolot, 2005). Full-waveform systems will record and recognize the returned signal based on fixed intervals, while the discrete return system used in this study, is usually capable of identifying a maximum of five return signals per pulse.

Full-waveform systems are preferred when covering larger areas. Usually the footprint size is considerably larger than discrete return systems. Full-waveform are usually used to measure stand heights, aboveground biomass, and basal area. Lefsky et al. (1999a and 1999b) studies, where full-waveform was the primary tool used to understand the forest structure, focused on the prediction of aboveground biomass.

Focusing on the discrete-return systems, Naesset (1997b) was able to estimate timber volume, and extract forest information aiming the studies more at an individual tree level. The author was able to explore studies where tree heights and number of stems were estimated (Naesset et al., 2001), acquiring crown information such as height to the crown and average relative crown length (Naesset et al., 2002), and predicting many other forest characteristics such as basal area, and volume (Naesset 2002). The tree height prediction was computed from the LiDAR data assuming that the last return of each LiDAR pulse was a ground hit, and all the remaining points were vegetation. Having this information, the author was able to extract heights by subtracting the vegetation points from the ground.

An interesting characteristic of LiDAR discrete-return system is a “dead zone” between pulse echoes, which represents the capability of a multiple return sensor to detect and record the next echo after the previous echo. This zone usually ranges between 2 m and 7 m in vertical length (Nayegandhi et al., 2006). Another definition of this characteristic is the “temporal resolution” of the sensor.

The wavelengths used by these sensors typically cover the range of 900-1064 nm, where the energy from reflected vegetation is high. While longer wavelengths are less affected by atmospheric noise, LiDAR cannot be considered an all-weather system and is typically flown under clear sky, cloud free conditions (Lefsky et al., 2002). That does not mean LiDAR systems cannot be flown on days with clouds; the requirement then is to fly below the clouds.

With regard to vegetation, fewer pulses will reach the understory vegetation, or the terrain below, in areas where dense canopy cover is present. Takahashi et al. (2006) tested the penetration rates of two species of cypress (Sugi cypress and Hinoki cypress) with low canopy openness. Fewer gaps in the tree canopies affected the degree to which LiDAR pulses were able to penetrate the tree structure. This resulted in a lower resolution DTM and also in less precise data describing understory vegetation.

### 3.1 – Remotely-sensed data and individual tree identification

It is crucial to acquire precise and accurate data to better understand the forest structure. Identifying individual trees with remotely-sensed data is a step that improves the understanding of a forested system considerably. Individual tree identification is a well-known topic in the scientific research. One can find many examples in the literature describing different methods tested, and applied, to identify individual trees in forested areas. There are a variety of the different remotely sensed datasets used to accomplish the tree identification such as: air-photos (Dralle et al., 1997; Larsen et al. 1997; Wolf et al., 2007), multi-spectral sensors (Gougeon et al., 2006, Katoh et al. 2008), and LIDAR. The

objective of this section is to highlight some of the different methods and datasets used for the identification of individual trees.

Dralle et al. (1996) used scanned aerial photos to estimate the number of individual trees in a forested area. The method implemented in this study presented two major steps: smoothing the digital images first, and estimating the number of treetops above a threshold. The smoothing step applied a low-pass filter to decrease the amount of spurious data. In other words, the filter was used in an attempt to remove multiple treetops sometimes found representing a single tree canopy. The condition where this situation arises is when the data resolution is much finer than the object crown size. After applying the filter, the mode of pixel values was calculated for the study area and used as a threshold to ignore potential treetops below that value.

There are many factors that might cause multiple treetops in a tree canopy, such as broken treetops, overlapping tree canopies, or minor variations in image intensity. The same issue was identified by Larsen (1997), where crown models were used as templates to estimate the location of individual trees. Once again, high-resolution aerial photos were used taking into account light source characteristics (sun angle and shadows), camera angles, and flight direction.

A more simplified and faster method to identify individual trees using aerial photography was shown by Niemann et al. (1999) by using 1 m resolution digitized photos. This study assumed that a treetop represents the brightest spot in a tree canopy and that its surroundings will have lower values. A roving 3 pixel by 3 pixel window was moved incrementally over the digital image, searching for the local maxima within the window.

Once the maximum value is represented by the central pixel of the search window that cell is marked as a treetop. Employing the same idea of a moving local maxima window and identifying individual treetops, Wulder et al. (2000) used multi-spectral imagery and variable window sizes to improve the identification of trees. Also using the local maxima idea, Maltamo et al. (2003) were able to identify individual treetops using digital video imagery. The technique was applied on enhanced digital images produced from the original video overlapping frames.

The next step in the individual tree detection is the canopy delineation of the tree in question. Gougeon (1999) delineated crowns using techniques such as thresholds to mask undesired vegetation layers, local minima to identify the crown edges, a valley-following approach connecting local minima, and pixel-based guided rules within edges. Brandtberg et al. (1998) developed a multi-scale automated method to delineate tree crowns by identifying the zero-crossings in the second derivative of the image (edge detection). Uuttera et al. (1998) applied the same idea of edge detection, where after smoothing the aerial images, the Laplacian filter was applied to enhance the desired features (crown edges). Culvenor (2002) used a similar approach to Gougeon (1999) to delineate Eucalyptus trees, where local maxima and minima were involved in the process of identifying the treetop (seed points) and valleys between trees.

More recent papers use higher spatial resolution datasets, bringing new challenges to the tree delineation, because more detail is introduced to the datasets as well as noise. This is the case of Wu et al. (2004), where airborne imagery with a spatial resolution of 10 cm was used. The algorithm developed attempts to use the difference between intensity and

saturation channels to delineate canopies in three main scenarios: city, dispersed trees beside highways and dense tree in a forest. Results showed that city scenarios had the best success in delineating canopies and that the increase in tree density lowered the accuracy of delineation. Another example of a recent study using high-spatial resolution imagery is Katoh et al. (2008), where a multi-spectral sensor was used to collect data providing images with 50 cm of resolution after correction. The authors used the method implemented by Gougeon (1999), where a valley-following algorithm was used to delineate the tree canopies.

Advances in technology bring the development of new tools with higher spatial resolution such as the LiDAR systems. With little data manipulation, LiDAR datasets are able to provide crucial information about a forest: tree heights. Also, these systems bring the opportunity of collecting information throughout the different layers of vegetation by being able to provide multiple returns for a single pulse (Lim et al., 2003; Clark et al., 2004). The next chapters will demonstrate the LiDAR technology being used in different sectors of research, and focusing later on individual tree identification.

### 3.2 – Computer algorithms for LiDAR data

With the introduction of LiDAR sensors and datasets for commercial purposes, the development of public and private tools for the extraction of information about topography and forestry increased drastically.

Vertical and horizontal forest structure is highly dependent on topography, thus influencing the amount of water, light, and nutrients available for the vegetation. Tree species will benefit differently from these different types of habitats according to the availability of these natural resources. Many studies focus on using LiDAR as the main data source for the creation of DTMs. Computer algorithms have been developed to create DTMs such as the algorithm developed by Kraus and Pfeifer (1998) where the LASER points cloud is separated into ground points and non-ground points using weights attached to each LASER point depending on the vertical distance between the expected DTM level and the corresponding laser point. Also, Vosselman and Maas (2001) developed a slope-based filtering technique using mathematical morphology for the creation of DTMs. Zhang et al. (2003) developed a progressive morphological filter ("erosion", "dilation", and "opening" mathematical operations) with a varying size of the window filter to identify non-ground points and remove them from the final dataset, allowing for the creation of a DTM.

DTMs derived from LiDAR data allow for the extraction of meaningful information on environment variables influenced by topography. Using image segmentation and LiDAR data, Cobby et al. (2001) developed numerical flood models able to differentiate between floodplain environment components such as rivers and short or tall vegetation.

LiDAR data have also been used to examine temporal changes in vegetation cover. This is shown in the work of Yu et al. (2004), where an algorithm was developed to identify harvested trees. Using LiDAR data collected in different years, the authors created a

CHM for each dataset. These multitemporal CHMs were overlaid and subtracted, resulting in an image showing the difference in vegetation between the years.

### 3.3 – LiDAR data and individual tree identification

In the forest sector, computer algorithms have been developed to better understand the surrounding ecosystem, the topography of watersheds, and forest characteristics, such as tree height and forest cover. This section will provide more information about studies where the main objective was the identification of treetops and canopy delineation using computer algorithms.

Andersen et al. (2001) used mathematical morphological techniques to identify tree apex locations using grayscale LiDAR data. Using a user-specified grid cell size, it was possible to filter the raw LiDAR data and extract the highest value for each cell. With the filtered dataset, a DSM was created and used for the morphological analysis called "opening". "Opening" is the sum of "erosion" and "dilation", where first the image is eroded and dilated in sequence. For this process there is always a structure element, with any size and shape, which guides pixel by pixel the processing throughout the image. Dilation will expand an object in the image adding adjacent pixels to it, while erosion will shrink the object by removing adjacent pixels. Basically, applying an opening technique will remove parts of the image that are smaller than the structure element. For the LiDAR data, the structure element used was a disk with varying sizes and the parts removed were the treetops.

Popescu et al. (2002) developed an algorithm to identify the top of the trees using variable local maxima windows. A local maximum was identified where the magnitude of the digital number (in this case the height of the vegetation) is greater than the surrounding neighbours (Wulder et al., 2004). The final result is an image with the top of the trees identified. With these data, it is possible to extract accurate information of individual trees such as height, location, or estimation of the number of trees in a given area.

Koch et al. (2006) developed an algorithm to detect and delineate individual tree crowns using LiDAR data. Using rasterized DEMs and DSMs derived from LiDAR data, the authors were able to create digital canopy height models for their study areas. These CHMs were then used as datasets for the developed algorithm. Gaussian filters were used to minimize multiple treetops for a single tree and gaps in between canopies were filled with data in order to avoid edge effects. Local maximum filters were used for identifying individual treetops, where a pixel was counted as a treetop if all the surrounding pixels were lower than its height. For canopy delineation, the authors used different methods trying to reflect the best shape of the tree canopy. First, a "pouring" algorithm (implemented in the MVtec HALCOM software package) was used. This algorithm resembles a watershed algorithm: starting from the treetop identified before, the code keeps looking for the valley-bottom (Diedershagen et al., 2003). This algorithm provides preliminary canopy delineation and in sequence the authors applied sets of pre-defined threshold to slightly adjust the tree canopies.

Identifying trees and delineating crowns with LiDAR datasets means working with an enormous amount of data. Newer LiDAR systems with higher frequency and pulse rating can even provide an increased number of returned points per square metre. The easiest path when working with such high amount of data and trying to identify treetops is gridding the LiDAR dataset into a raster image. Treetops will be represented by the brightest pixels in the image. Studies have been carried out exploring this idea (Persson et al., 2002; Matsugami et al., 2005; Chen et al., 2006; Kwak et al., 2007) and applying user-specified kernel sizes, with treetops being identified by local maxima.

Raw LiDAR data were chosen over gridded raster datasets in order to avoid gridding the datasets and searching for bright pixels to identify treetops. The raw LiDAR data are composed of every returned pulse captured by the sensor and it is then classified into two classes: ground pulse and non-ground pulse. By using raw data, subtle changes in a single tree crown can be observed, therefore enhancing the results envisioned by this study. Raw datasets are a unique challenge for this study, increasing the amount of information to be processed by the proposed computer tools. The goal will be the development of tools that can provide accurate, precise and fast information about the forest structure. The approach of using raw LiDAR datasets, and the development of these tools for canopy characterization are described in the following chapters.

# Chapter 4: Study Area

## 4.1 - General Description

The study area is located in the Greater Victoria Water District, situated west of Victoria, B.C., Canada. Established in 1942, it includes two main protected watersheds (covering more than 11,000 ha): Sooke and Goldstream. Watershed areas are important in capturing most of the drained water of rain or snow and funnelling it downhill into rivers, creeks, wetlands or dams. The water from the watersheds is stored in Sooke lake and other small reservoirs. Concerns about forest fires in the watersheds are taken seriously, specially because fire can diminish the amount available and quality of the stored water. Logging was still allowed in the area 15 years ago. However, it has since been prohibited due to concerns regarding water quality and ecosystem health

The area presents a variety of terrain types, stand ages, and structures, making it a perfect study area for testing the different modules of the software to identify trees and their canopies. The most common tree species assemblage in this valley is Douglas-fir (*Pseudotsuga menziesii* (Mirb) Franco)–western hemlock (*Tsuga heterophylla* (Raf.)). Less common tree species in the area are: Western Redcedar (*Thuja plicata*), White Pine (*Pinus monticola*) and Alder (*Alnus rubra*).

## 4.2 - Rithet Creek Valley

### 4.2.1 - Rithet Creek

A specific area in the Sooke watershed, Rithet Creek valley was chosen for the collection of ground data (Figure 2). The elevation in the valley varies between 190 and 840 m being mostly dominated by moderate to steep hills. There are many small creeks that contribute to the flow of Rithet Creek, which pours all the contributed water into the Sooke reservoir.

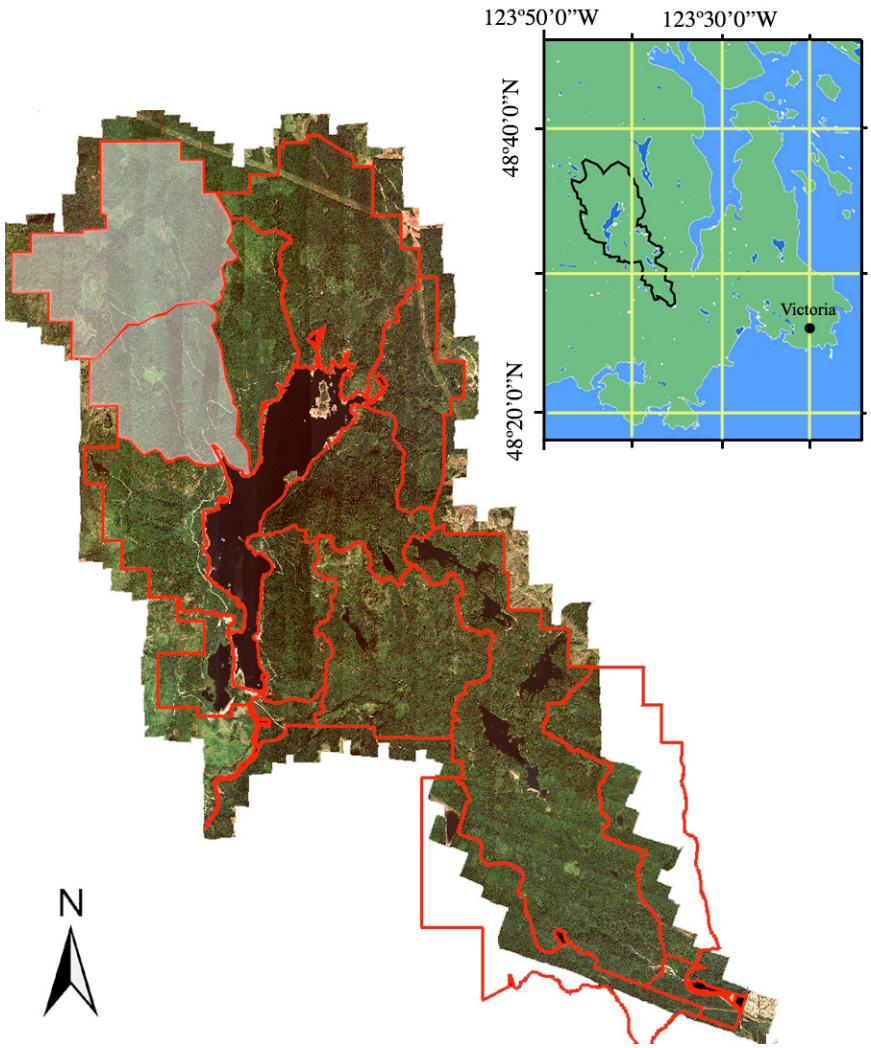


**Figure 2 - Location of the study area. Individual watersheds within the CRD water land base (red boundaries). Shaded area represents the study area, Rithet Creek valley.**

### 4.2.2 - Dominant Tree Species

The valley forest composition was strongly influenced by the fires that had occurred in the past. Because of their thick bark, Douglas-fir trees are able to withstand high temperatures during a forest fire. This special species characteristic made Douglas-fir the most common tree species found in the study area. Furthermore, Douglas-fir is a fast growing species with its canopy located towards the top, making it harder for fire to reach the crown. There are also other species in the area, occurring in lower frequencies when compared to Douglas-fir, such as: Western Hemlock, Western Red Cedar, White Pine, and Alder. Because Douglas-fir is the dominant tree species in the Sooke Watershed, and most importantly because it is the dominant species in the study area, special attention will be given to this coniferous tree and the detection of its apex and delineation of its crown.

## 4.3 - Douglas-fir and a digital form

Understanding tree structure (morphology) improves the development and performance of an algorithm for handling treetop search and crown delineation. LiDAR pulses that penetrate in the different levels/layers of the tree canopy interact with tree components (needles, branches, bark, etc.) being forced to diverge, refract or simply continue to penetrate deeper into the canopy and interact with other components. Most of the pulses that reflect back to the LiDAR sensor will be used to represent (after pos-classification) crown points, understory vegetation, and/or bare-earth terrain.

The algorithm must recognize crown points that fall within the tree crown area projected on the ground (Figure 3). Douglas-fir crowns are not perfectly cone-shaped. Usually, multiple treetops can be identified within a single crown. This is because many branches are oriented towards the top, creating what will be called here "pseudo-small apexes". This is one of the greatest obstacles for the algorithm to overcome because the delineation of the canopy can incorrectly identify the edge of the canopy.

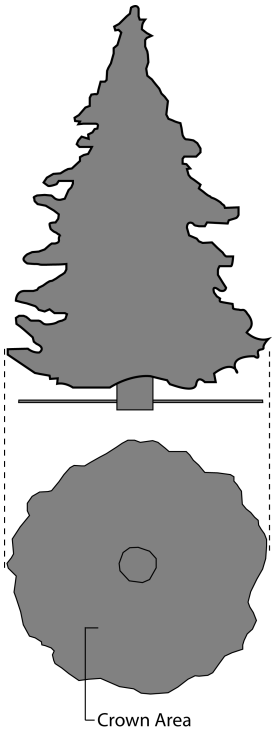


**Figure 3 - Projected crown area on the ground.**

# Chapter 5: Methods

This chapter introduces all the processing steps that the LiDAR dataset followed to create the final outputs (individual treetops identification and canopies delineation).

## 5.1 - LiDAR data

The LiDAR sensor was mounted on a helicopter and the dataset was collected in the summer of 2004. The sensor had a pulse frequency of 50KHz at a flying height of 800 meters above ground level, resulting in an average posting density of 4.7 points/$m^2$.

Preliminary data cleaning was carried out after the data acquisition, focusing on the removal of noise from spurious heights, due primarily to atmospheric effects. Subsequently, the data were classified using the Terrascan software (Terrasolid Corporation, Jyväskylä, Finland), where LiDAR return points were discriminated into two categories: ground points and vegetation points.

## 5.2 – Data collection

During the summer of 2005 data were collected in the study area for testing the accuracy of the algorithm. Nine plots were dispersed throughout the area, located to represent the different tree species and tree ages as best as possible (Table 1). Three broad age classes were chosen to represent the area: Young growth (Figures a-c) - 1-20 year old trees, 0-17 m tall; Intermediate growth (Figures d-f) - 21-40 year old trees, 19-33 m tall; and Old growth (Figures g-i) - 141-250 year old trees, 55-65 m tall.

| Young-Growth Plots<br><br>Plot 3 (a), Plot 6 (b),and Plot 9 (c) | Intermediate-Growth Plots<br><br>Plot 1 (d), Plot 4 (e), and Plot 7 (f) | Old-Growth Plots<br><br>Plot 2 (g), Plot 5 (h), and Plot 8 (i) |
|---|---|---|
|   |   | 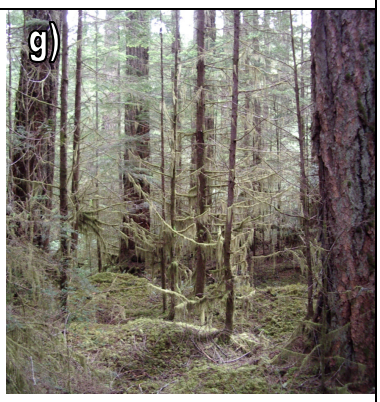  |
| 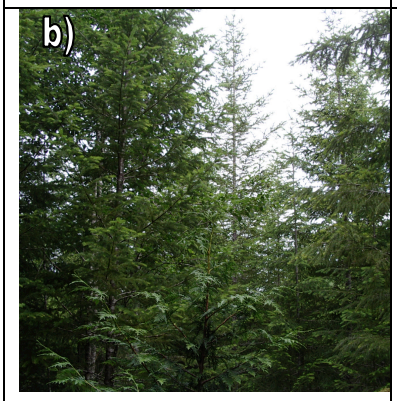  |   | 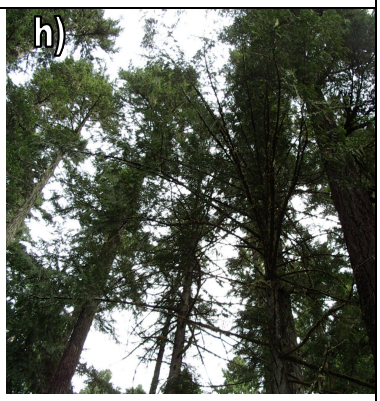  |
|   |   |   |

**Figure 4 - Photos showing in more details the distribution of trees within plots.**

**Table 1 - Details about the nine surveyed plots.**

| Plot # | Size | Age Class | # of Trees | Dom. / Co-Dom. | Percent (%) |
|---|---|---|---|---|---|
| 1 | 40 x 40 m | Intermediate Growth | 268 | 59 | 22.0 |
| 2 | 40 x 40 m | Old Growth | 207 | 12 | 5.8 |
| 3 | 20 x 20 m | Young Growth | 59 | 20 | 33.9 |
| 4 | 40 x 40 m | Intermediate Growth | 183 | 71 | 38.8 |
| 5 | 40 x 40 m | Old Growth | 97 | 17 | 17.5 |
| 6 | 20 x 20 m | Young Growth | 241 | 34 | 14.1 |
| 7 | 40 x 40 m | Intermediate Growth | 144 | 87 | 60.4 |
| 8 | 40 x 40 m | Old Growth | 74 | 20 | 27.0 |
| 9 | 20 x 20 m | Young Growth | 76 | 26 | 34.2 |

Stem maps were produced for each of the plots. Along with the location of the stems (Appendix A), tree species were identified, selected tree heights, diameter at breast height (DBH), height to living crown (HLC), and crown radius were measured, and tree dominance in the plot was assessed (based on the criteria: “suppressed”, “intermediate”, “co-dominant” and “dominant”). DBH was measured using a caliper with adjustable jaws; the measurements were acquired in centimetres and recorded in a portable handheld computer. The “dominant” nomenclature was used to classify trees whose canopies were not suppressed, or obscured by any other tree canopies. From a bird's eye view, the dominant trees were the most visible and distinguishable canopies (Figure 5).

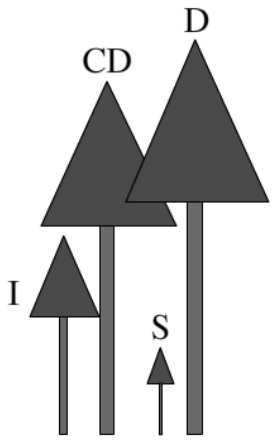


**Figure 5 - Tree dominance: D – dominant trees; CD – co-dominant trees; I – intermediate trees; and S – suppressed trees.**

The "co-dominant" class was used to classify trees that were almost as tall as the "dominant" trees, but with part of their canopies shaded by the "dominant" trees. Trees below the "co-dominants" but with heights greater than half of the "co-dominant" and "dominant" trees were classified as "intermediate". Small trees below the "intermediate" were classified as "suppressed". These trees suffer from strong competition for light and nutrients with the surrounding taller trees.

All the "dominant" and "co-dominant" tree heights were included for each plot. A LASER rangefinder was used to survey the heights. Not all the "suppressed" and "intermediate" tree heights were measured. The most important objective of the height measurements was to collect details on the trees that were easily identifiable on the LiDAR data. These trees were the "dominant" and "co-dominant" trees. "Suppressed" and "intermediate" tree heights were also acquired but in fewer numbers and were chosen randomly.

For the trees that were not surveyed for height, allometric models using measured DBH and height for each dominant category were developed. The power model was the best predictive model observed for the plots in study. Table 2 presents the observed $R^2$ and coefficients for the predicted models. Also, figures 6-8 present the charts for each category of surveyed plot with the proper model equation.

**Table 2 - Plots statistics.**

Dependent = Height (m)
Independent = DBH (m)

| PLOT | $R^2$ | d.f. | b0 | b1 |
|---|---|---|---|---|
| Young growth | 0.9009 | 82 | 38.162 | 0.6985 |
| Intermediate growth | 0.8900 | 380 | 76.991 | 0.9057 |
| Old growth | 0.9203 | 95 | 53.787 | 0.8226 |

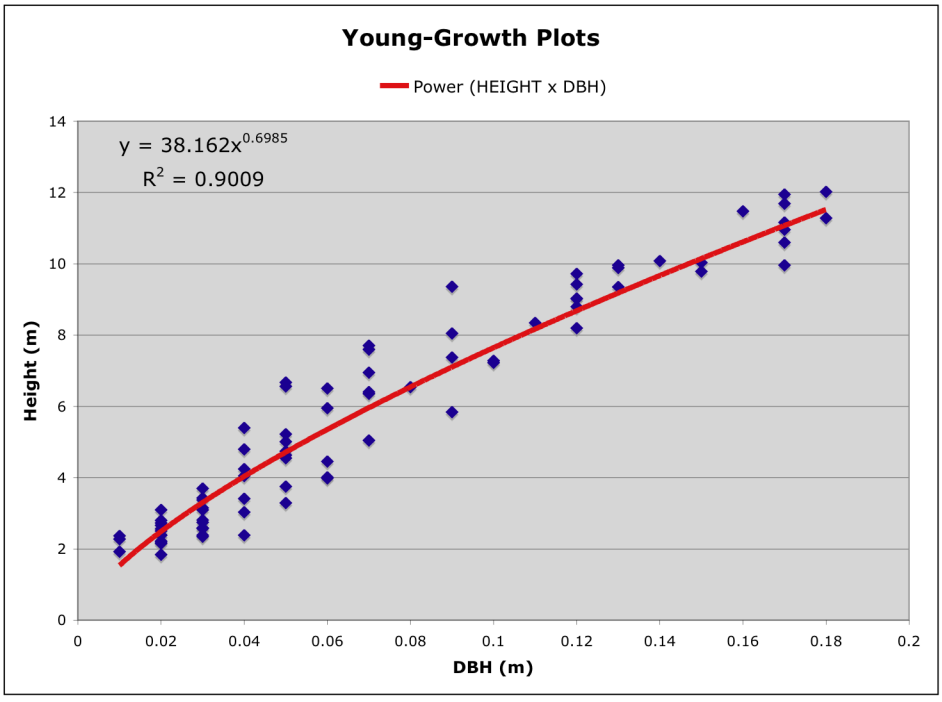


**Figure 6 - Height vs. DBH for young-growth plots.**

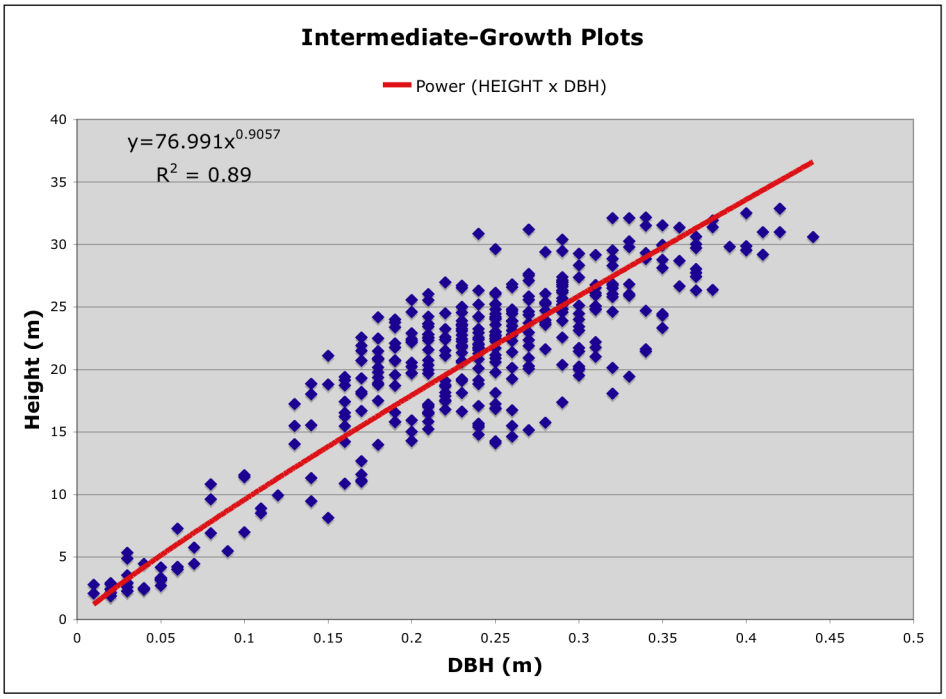


**Figure 7 - Height vs. DBH for intermediate-growth plots.**

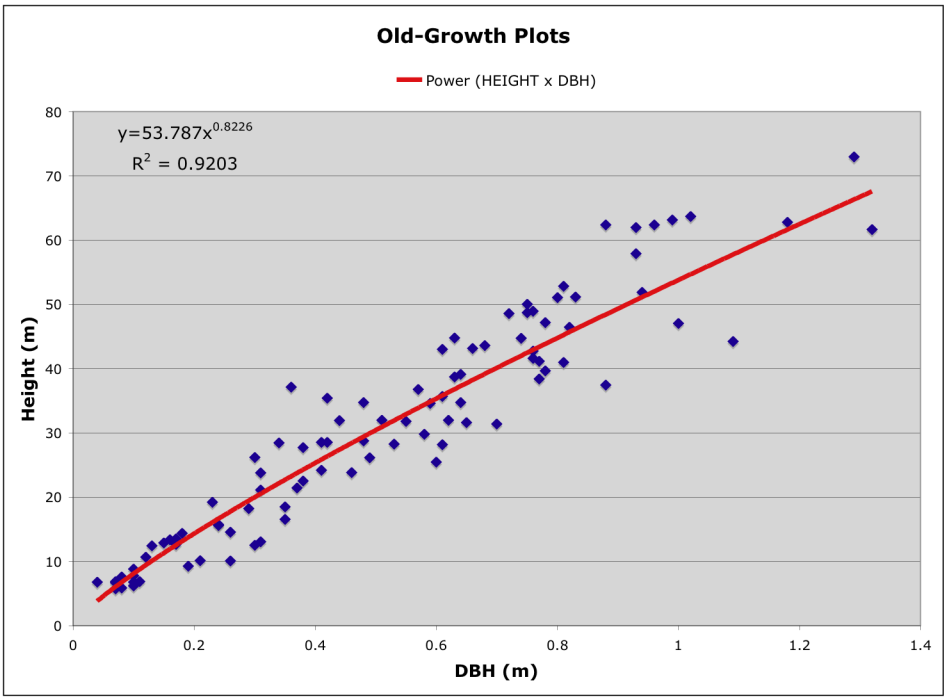


**Figure 8 - Height vs. DBH for old-growth plots.**

## 5.2 – Processing the LiDAR data for treetop identification and canopy delineation

### 5.2.1 - Extracting ground and vegetation points

The first step of the individual tree identification was to create different files containing only ground and vegetation. A simple routine was developed to search the ASCII files for different class identifier numbers. In the original ASCII files, ground points had a class identifier number equal to "2" and vegetation received the value "1". The routine created two new files for each original file (Figure 9): one ground file and one vegetation file.

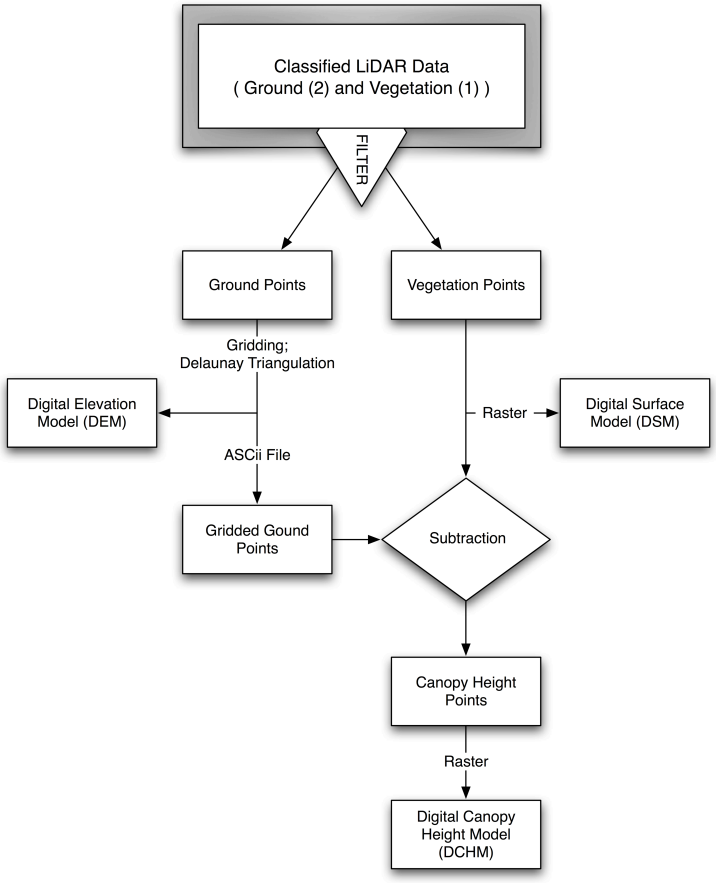


**Figure 9 - Flowchart displaying steps for creation of CHM.**

### 5.2.2 - Gridding the ground

Having the ground points in separate files made it more efficient to create a gridded ground model with a user specified resolution. In a vegetated area, a ground file will always have fewer points than the vegetation file. This was influenced by many different physical variables, but mainly by the fact that there were fewer LiDAR returns captured by the sensor for the ground than for the vegetation. Examples of physical problems could be: dense canopies, where the LiDAR pulse might have never reached the ground cover, or the intensity of ground return might have been really low, not being captured by the sensor, or disturbances in the atmosphere, such as dense clouds.

Analyzing the classified ground LiDAR points, it was observed that there was an average of one LiDAR point per square metre. Having this information, it was assumed there was little topographic variation in small cell sizes, so a 2 m spatial resolution was chosen for gridding the ground points. The objective of gridding the ground was to create a DEM and to reduce the file size of ground points file, making further data manipulation easier and faster. Gridding ground points required two separate steps, where the first was to construct a Delaunay Triangulation of a planar set of the ground points. Triangulation was a necessary step for gridding ground LiDAR data, especially in dense vegetated areas where LiDAR returns of the ground might be missing (Figure 10c).

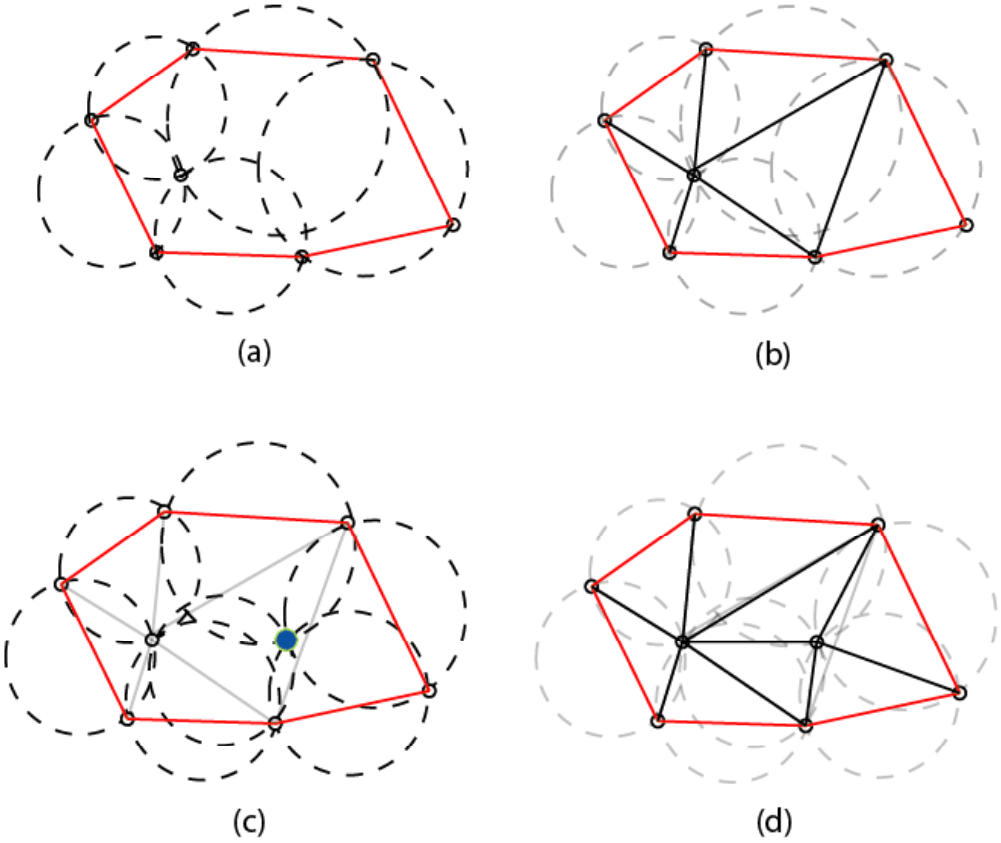


**Figure 10 - Simple example of triangulating some LiDAR ground points. (a) shows the circumcircles being added around points. A triangle will be a valid triangle if and only if a circumcircle holds no other point of the point set. (b) shows the points connected, creating the triangles. (c) shows the method where a point is added in the set of points and new circumcircles being examined. (d) shows the new triangles formed after the newly added point. The red line represents the convex hull that contains all the ground points.**

After triangulating the set of points, a regular grid was created to accommodate the new ground points. These points represented coordinates gridded to the specified spatial resolution (2 m). The final result, the DEM (Figure 11), represented the relief of the study area.

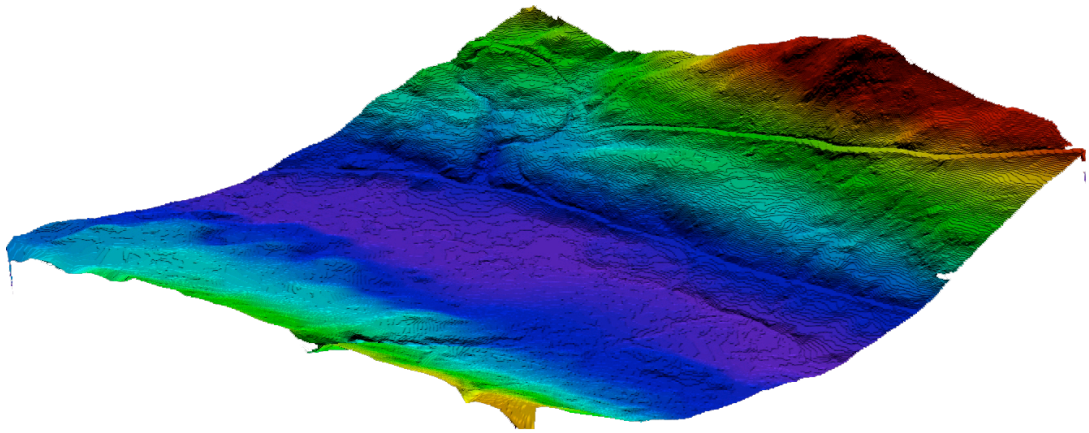

**Figure 11 - DEM with resolution of 2 x 2 m after gridding process**

### 5.2.3 - Vegetation file

The classified vegetation points were contained in a separate ASCII file. These vegetation points represented the LiDAR pulses reflected from any non-ground surface, being either understory vegetation or trees. Many reflected returns acquired by the sensor relate to the same tree, but representing hits from the lower branches, the stem, or the treetops.

One of the goals of this project was to retain the vegetation points in an unaltered format. The vegetation ASCII file containing all the vegetation return points did not receive any treatment, i.e., the data were not gridded (no interpolation methods applied), nor were any smoothing filters applied. As such, no information was lost, however the resulting file sizes were large, generally containing millions of points.

For visualization, a DSM (Figure 12) was created from the vegetation file. This DSM represented the vegetation that exists in the area but with the influence of the topography. In other words, each vegetation Z value represented the height of the tree added to the elevation of the terrain (elevation above sea level).

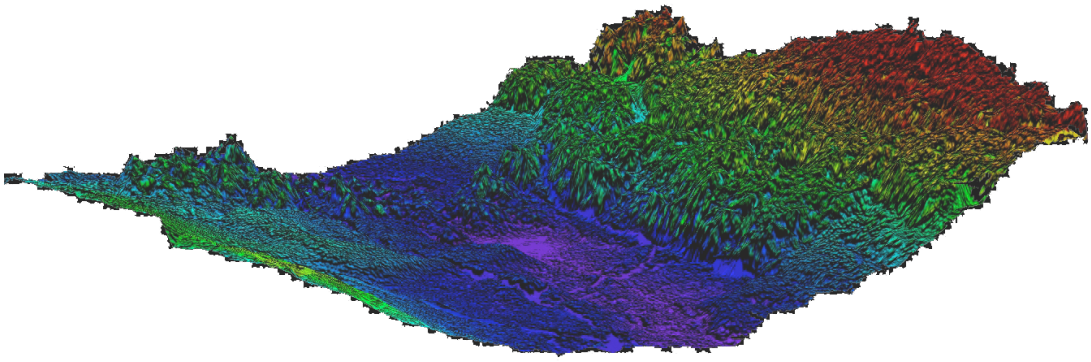

**Figure 12 - DSM created with vegetation points extracted from the LiDAR data.**

### 5.2.4 - Subtracting the DEM from the vegetation points

With the gridded ground and the vegetation raw points it was possible to start the creation of a CHM. The CHM output represented the actual tree height, without the influence of the terrain. Vegetation points that fell within a gridded ground cell were subtracted from the averaged elevation height of that cell. It was possible to identify the vegetation points that fell within each cell as each point had its own UTM coordinates. Figure 13 is displayed below for a better understanding of the subtraction procedure.

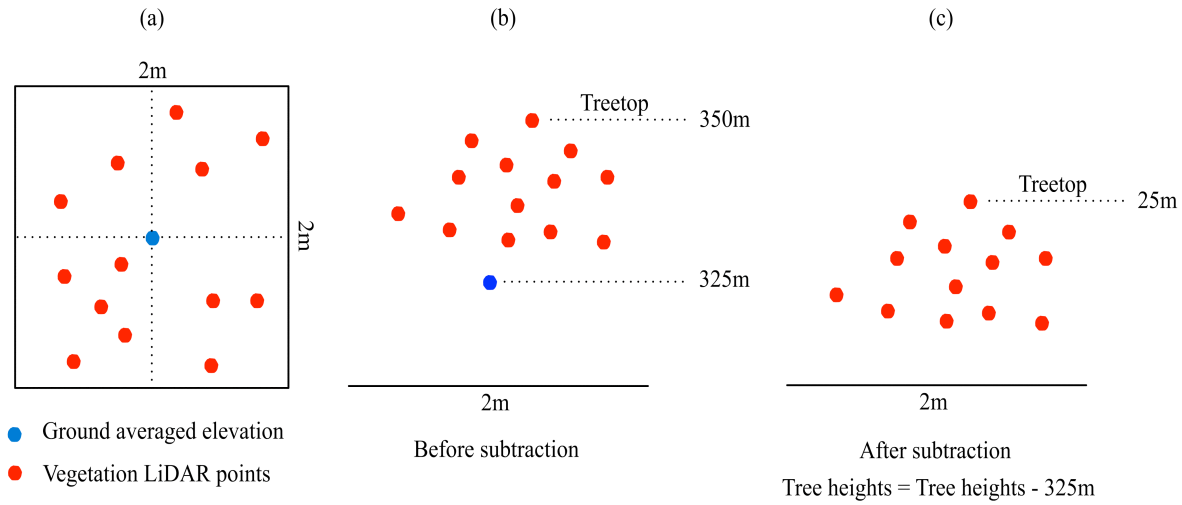


**Figure 13 - Subtraction procedure. (a) Birds-eye view of ground cell. (b) Side-view of LiDAR points within cell. (c) Tree heights without elevation effect.**

The subtracted file contained all the original vegetation points but now without the topography. It was still considered a "raw" file because it contained the individual LiDAR points, and had not undergone additional processing such as gridding or interpolation. With the newly created CHM it was possible to start the individual tree detection, as now the treetops and canopies were more distinguishable (Figure 14).

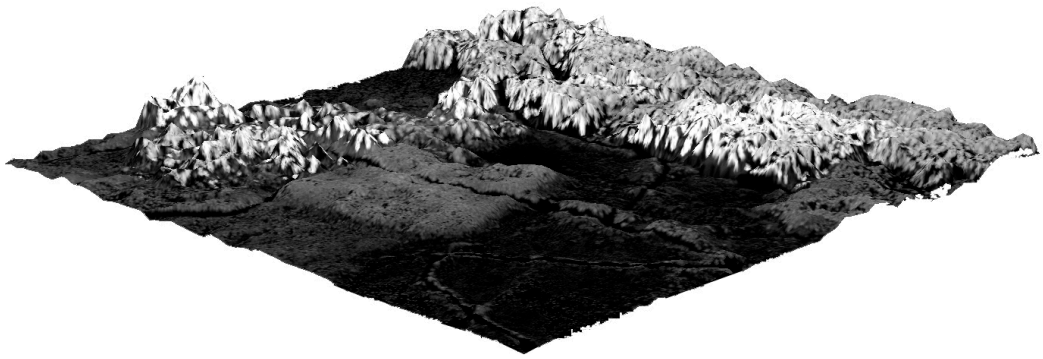

**Figure 14 - CHM created after subtracting the DEM from the DSM.**

### 5.2.5 - Treetops detection and canopy delineation algorithm

The developed algorithm was intended to be as simple as possible for the user, who had only to supply the algorithm with the LiDAR point data. The data needed to be formatted as ASCII files containing the UTM coordinates and the elevation in metres for each return pulse. The algorithm provided two outputs: treetop coordinates and vector files for the delineated canopy. The first output, showing the position of each treetop, was formatted as ASCII files and contained three columns: the UTM coordinates, easting and northing, and the height in meters for the treetop. The second output file was a binary vector file for each tree canopy delineated. This file was formatted as an ENVI binary vector.

#### 5.2.5.1 - Setting global variables

A few variables were defined at the start and stored in memory. These were constant values that were chosen with the help of field data, making the code more stable for the desirable study area. The first variable was a height threshold, where all the LiDAR points below the threshold value would be ignored. The default was typically set to 2 metres (Naesset, 1997a). Anything below this threshold was considered understory vegetation, for example salal (*Gaultheria shallon*), a common shrub present in the area that reached average heights of 1.5 m.

For the algorithm to delineate tree canopies it was important to declare two other variables: the minimum and maximum radii for canopy crown size. These values represented thresholds in metres for the canopy edge detection. The algorithm did not

allow for canopy edges that were smaller than the minimum, and greater than the maximum, radius. The minimum radius was typically set to 1 m, as this value represented the minimum crown radius for the dominant trees surveyed in the field. The maximum radius value existed only as an upper threshold, in order to ensure that there were no canopy edges greater than the maximum radius surveyed in the field. This variable changed from stand to stand. The user had the option to choose between three stand types: young, intermediate, or old-growth plots. For young plots, the maximum radius would be 2 m, based on field data. Intermediate growth plots had this variable set to a maximum radius of 3 m, and old-growth received a maximum radius of 4 m.

#### 5.2.5.2 - The algorithm

After declaring the global variables the algorithm started the process of identifying treetops and delineating the crowns. A basic assumption made here was that every treetop was defined by the highest measured height. The code then searched for the highest value in the dataset. This first value represented the tallest tree in the dataset, and the tallest treetop in the area. Having this treetop UTM coordinate, the code then saved both positions (easting and northing) in memory, and the treetop height in metres.

For the delineation of a tree crown it was necessary to understand what the edge of a tree crown was. As will be described more fully later in this paper, an edge was defined as where two canopies interact when too close to each other, or the end of the canopy and the beginning of the ground. For the delineation, 36 iterations would result from the first

treetop. Each iteration represented an addition of 10 degrees in a clockwise search for the crown edges (Figure 15).

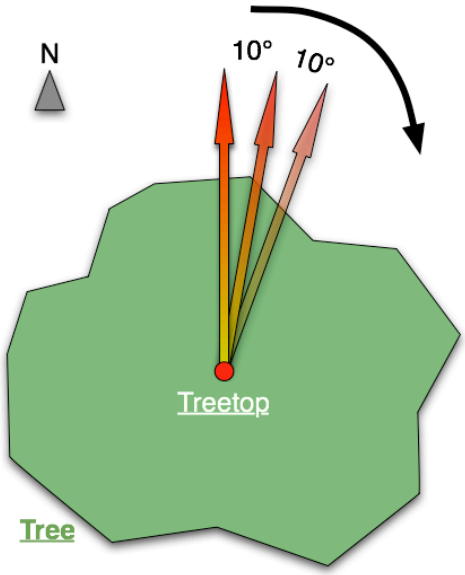


**Figure 15 - Clockwise addition of 10 degrees for every iteration.**

After the first treetop was located, it was crucial to understand exactly where to look for the crown edge. For every treetop there would always exist a tree crown edge to be delineated. The delineation always started at the north direction (0 degree). From this position the code calculated the UTM coordinates for "x" and "y" where the search had to come to a stop. Table 3 presents the calculation of the UTM coordinates for each iteration.

The equations used are shown below:

- $rad = \frac{\deg \times 2 \times \prod}{360}$, **Equation 1 - conversion of degrees (deg) to radians (rad).**
- $x = \cos(rad) \times radius$, **Equation 2 – X position**
- $y = \sin(rad) \times radius$, **Equation 3 – Y position**

**Nomenclature:**

TT_X represents the treetop easting position in metres;

TT_Y represents the treetop northing position in metres.

**Table 3 - Calculation of X and Y coordinates for every iteration.**

| Direction | Angle(clock.) | UTM +/- X (degrees) | UTM +/- Y(degrees) |
|---|---|---|---|
| **North** | 0 | TT_X | TT_Y + MAX(radius) |
| | 10 | TT_X + x(80) | TT_Y + y(80) |
| | 20 | TT_X + x(70) | TT_Y + y(70) |
| | 30 | TT_X + x(60) | TT_Y + y(60) |
| | 40 | TT_X + x(50) | TT_Y + y(50) |
| | 50 | TT_X + x(40) | TT_Y + y(40) |
| | 60 | TT_X + x(30) | TT_Y + y(30) |
| | 70 | TT_X + x(20) | TT_Y + y(20) |
| | 80 | TT_X + x(10) | TT_Y + y(10) |
| **East** | 90 | TT_X + MAX(radius) | TT_Y |
| | 100 | TT_X + x(10) | TT_Y – y(10) |
| | 110 | TT_X + x(20) | TT_Y – y(20) |
| | 120 | TT_X + x(30) | TT_Y – y(30) |
| | 130 | TT_X + x(40) | TT_Y – y(40) |
| | 140 | TT_X + x(50) | TT_Y – y(50) |
| | 150 | TT_X + x(60) | TT_Y – y(60) |
| | 160 | TT_X + x(70) | TT_Y – y(70) |
| | 170 | TT_X + x(80) | TT_Y – y(80) |
| **South** | 180 | TT_X | TT_Y – MAX(radius) |
| | 190 | TT_X – x(80) | TT_Y – y(80) |
| | 200 | TT_X – x(70) | TT_Y – y(70) |
| | 210 | TT_X – x(60) | TT_Y – y(60) |
| | 220 | TT_X – x(50) | TT_Y – y(50) |
| | 230 | TT_X – x(40) | TT_Y – y(40) |
| | 240 | TT_X – x(30) | TT_Y – y(30) |
| | 250 | TT_X – x(20) | TT_Y – y(20) |
| | 260 | TT_X – x(10) | TT_Y – y(10) |
| **West** | 270 | TT_X – MAX(radius) | TT_Y |
| | 280 | TT_X – x(10) | TT_Y + y(10) |
| | 290 | TT_X – x(20) | TT_Y + y(20) |
| | 300 | TT_X – x(30) | TT_Y + y(30) |
| | 310 | TT_X – x(40) | TT_Y + y(40) |
| | 320 | TT_X – x(50) | TT_Y + y(50) |
| | 330 | TT_X – x(60) | TT_Y + y(60) |
| | 340 | TT_X – x(70) | TT_Y + y(70) |
| | 350 | TT_X – x(80) | TT_Y + y(80) |

### 5.2.5.3 - The iterations

As described in the previous section, there were 36 iterations for every treetop and each iteration was a clockwise increment of 10° around that treetop. The delineation of a tree canopy did not happen instantaneously; there were a few steps involved before the code added a 10° increment and searched for the next canopy edge. The next paragraphs will go through the explanation of these steps.

With the UTM coordinates guiding the code as to where each iteration started and ended, the code connected these two points with a line. This line was an important guide because it determined which LiDAR return pulses belonged to that iteration. From these pulses, the code recovered the heights and determined where the crown edges were located. With the line as a geographical guide for direction and position, the code then set marks every 0.5m along the line. From these marks, the code then collected the position and height of the closest LiDAR pulse (Figure 16).

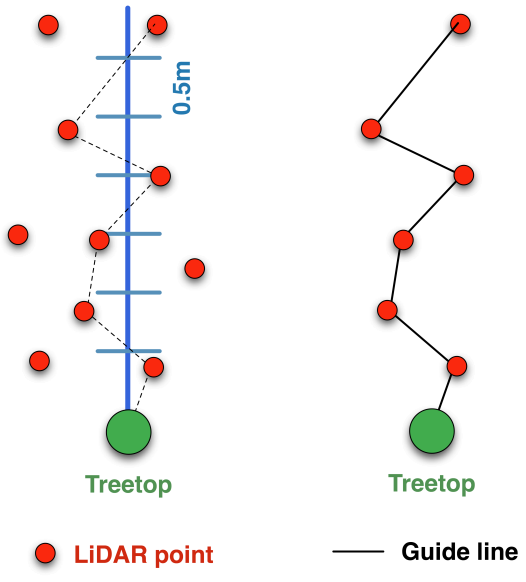


**Figure 16 - Example of the first iteration facing the north direction. The code searches for the closest heights for every 0.5 m mark.**

These first collected LiDAR pulses represented the new “line” facing the north direction. With all the heights collected, a search was then performed to detect the edge of the crown. To identify the edge, the algorithm checked for a "valley" between two trees, or if it was the end of the canopy and the beginning of the ground, also known as a “cliff" (Figure 17).

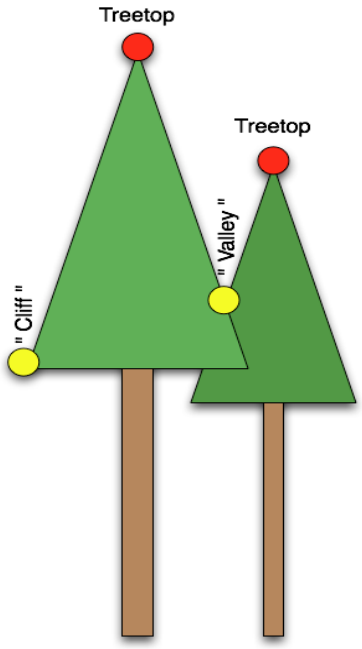


**Figure 17 - Showing the two situations the algorithm might handle; edges between two trees and edges between tree and ground.**

To identify a “valley”, the code checked every collected height on the extracted line. If the previous height was greater than the one being checked, and the subsequent height greater as well, then the height being checked was marked as the edge of the canopy for that iteration. Identifying a “cliff” was different from “valleys” because the code looked for a large discrepancy caused by a sudden change in height. If such a situation occurred, the code then recognized that the last point represented the edge of the canopy and stored

the coordinates and height of that point in memory. The code proceeded through all the 36 iterations, saving in memory all the identified edges for the subsequent steps of canopy delineation.

#### 5.2.5.4 – Vector files

When the algorithm reached the end of the 36 iterations it connected all the edge points stored in memory, building the first canopy shape. The output was then saved as an ENVI vector file. Figure 18 presents a flowchart with a concise explanation about all the processes involved for the treetop identification and canopy delineation.

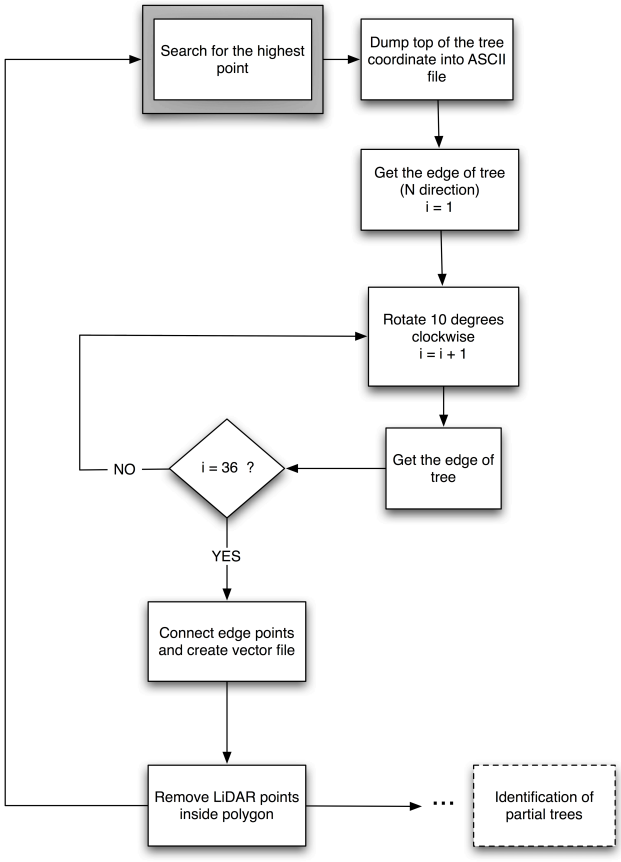


**Figure 18 - Treetop identification and canopy delineation algorithm flowchart.**

### 5.3 – Validation between field and algorithm coordinates

After identifying treetops, the next step was to validate their coordinates with field data. The code checked the identified tree position with the ones surveyed in the field. The input files for this algorithm were the field data and the ASCII files for the identified trees, with both datasets containing the UTM coordinates and tree heights. The code used the field tree positions as a starting point. From each field surveyed position it then calculated the minimum distance to every tree identified. The closest and tallest tree was marked as being the same tree surveyed in the field. A tree would not be marked if the minimum distance was greater than the radius threshold set by the user. This threshold was idealized as a buffer zone, representing a circular search area from the identified treetop with the same size as the maximum radius used to identify the "dominant" and "co-dominant" trees for each plot (global radius variables, sub-chapter 5.2.5.1). Figure 19 displays the extreme scenario of canopy shapes and their distribution in the field. In this example, the tree on the right is the first tree to run through the matching algorithm. This tree presents a crown that does not match a perfect idealized conical conifer crown shape because of competition for space and light with surrounding trees. This tree has basically no canopy on the west face, and also presents a displaced treetop from the centre. This displacement represents a tree with a broken crown.

The matching code also checked for difference in heights. If the absolute difference in height between field-measured and identified trees was greater than the height threshold calculated for each plot, the match was rejected (Figure 19). This height threshold calculation was developed based on the real field scenario. In dense and highly populated

plots, such as intermediate and old-growth plots, searching the treetops usually turned into a complicated task because of merging of neighbouring tree crowns with the one being surveyed. Visually, it was often very difficult, if not impossible, to locate the treetop inside the study-plot. To maximize the chance of visualizing the treetop, the distance between the survey instrument (LASER Rangefinder) and the tree, in intermediate and old-growth plots, was set roughly to the same as the tree height (Figure 20). In young-growth plots, where such merging of tree crowns was not present, the distance between instrument and tree was set to half of the tree height, this way avoiding wide angles.

Increasing the distance from instrument to the object maximized the chances of seeing the treetop. Even when increasing the distance there were still trees, where the surveyor would not be able to find the treetop location. In these situations a best estimate of the location was made. Therefore an extra tolerance step was added, in order to minimize the error caused by this approximation. A tolerance of ±5 degrees in the angle of sighting the treetop was added, providing a buffer in height for the matching algorithm.

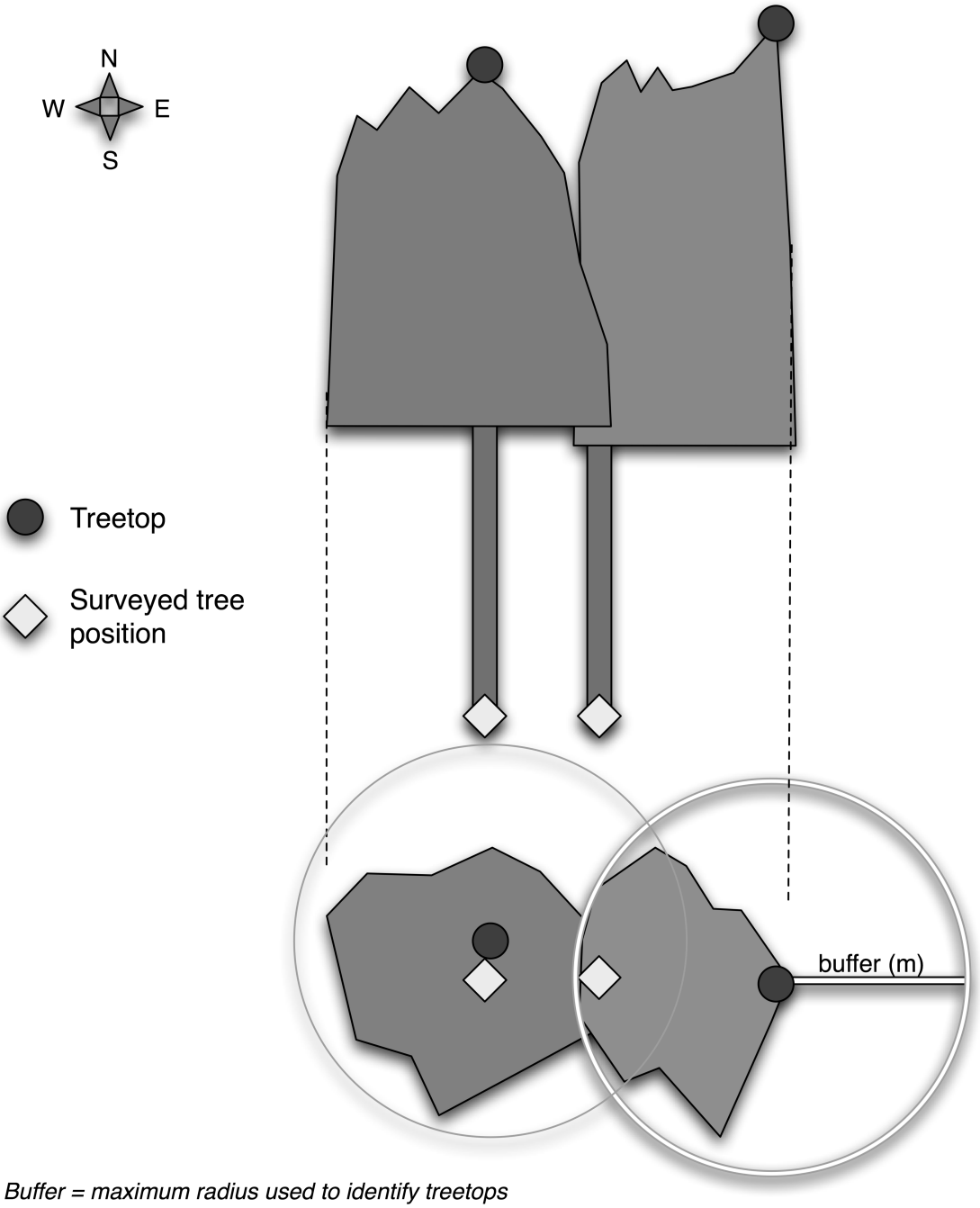


*Buffer = maximum radius used to identify treetops*
*Young-Growth buffer = 2 m*
*Intermediate-Growth buffer = 3 m*
*Old-Growth buffer = 4 m*

**Figure 19 - Matching treetops with field and algorithm data. Buffer size for the extreme case that might occur in the field.**

Young-Growth Plots

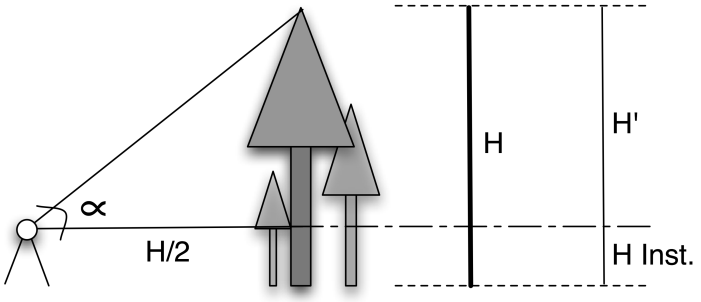


Intermediate & Old-Growth Plots

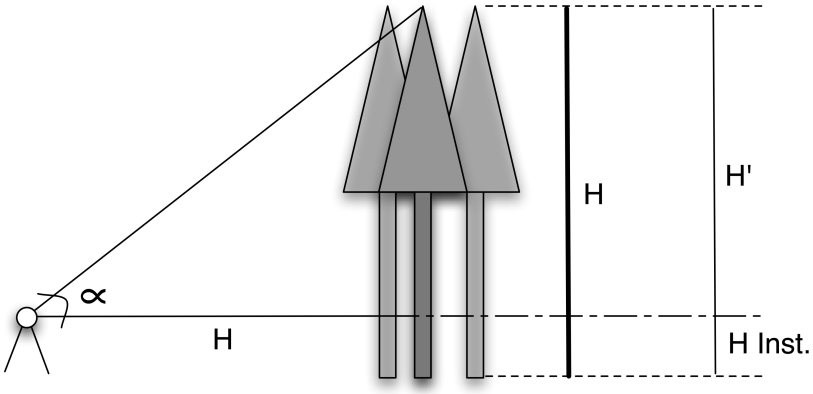


**Figure 20 - Height threshold calculation**

$\underline{Example}: H = 40m; Hinst = 1.5m$

$$\tan\alpha = \frac{(H')}{H} \Rightarrow \tan\alpha = \frac{(40-1.5)}{40} \Rightarrow \tan\alpha = 0.9625 \Rightarrow \underline{\alpha = 43.9^\circ}$$

$Adding \quad 5^\circ \Rightarrow \underline{48.9^\circ}$

$Subtracting \quad 5^\circ \Rightarrow \underline{38.9^\circ}$

$$\tan 48.9^\circ = \frac{(H'')}{40} \Rightarrow H'' = 1.1463 \times 40 = 45.85m \Rightarrow \Delta = 45.85 - 38.5 = \underline{7.35m}$$

$$\tan 38.9^\circ = \frac{(H'')}{40} \Rightarrow H'' = 0.8068 \times 40 = 32.28m \Rightarrow \Delta = 38.5 - 32.28 = \underline{6.22m}$$

$$\Delta Height = \frac{(7.35+6.22)}{2} = 6.79m \approx \underline{\underline{7m}}$$

Table 4 shows the averaged height thresholds calculated for each plot.

**Table 4 - Height thresholds used in matching algorithm.**

| Plot | Maximum tree height (m) | Delta height (m) |
|---|---|---|
| 1 | 31 | 5.2 |
| 2 | 70 | 12.0 |
| 3 | 17 | 3.3 |
| 4 | 41 | 7.0 |
| 5 | 50 | 8.6 |
| 6 | 11 | 2.0 |
| 7 | 27 | 4.5 |
| 8 | 53 | 9.1 |
| 9 | 10 | 1.8 |

Figure 21 demonstrates in more detail the steps involved in the matching algorithm. It shows the calculations involved in the different tolerance steps and also the global variables used for the different plots.

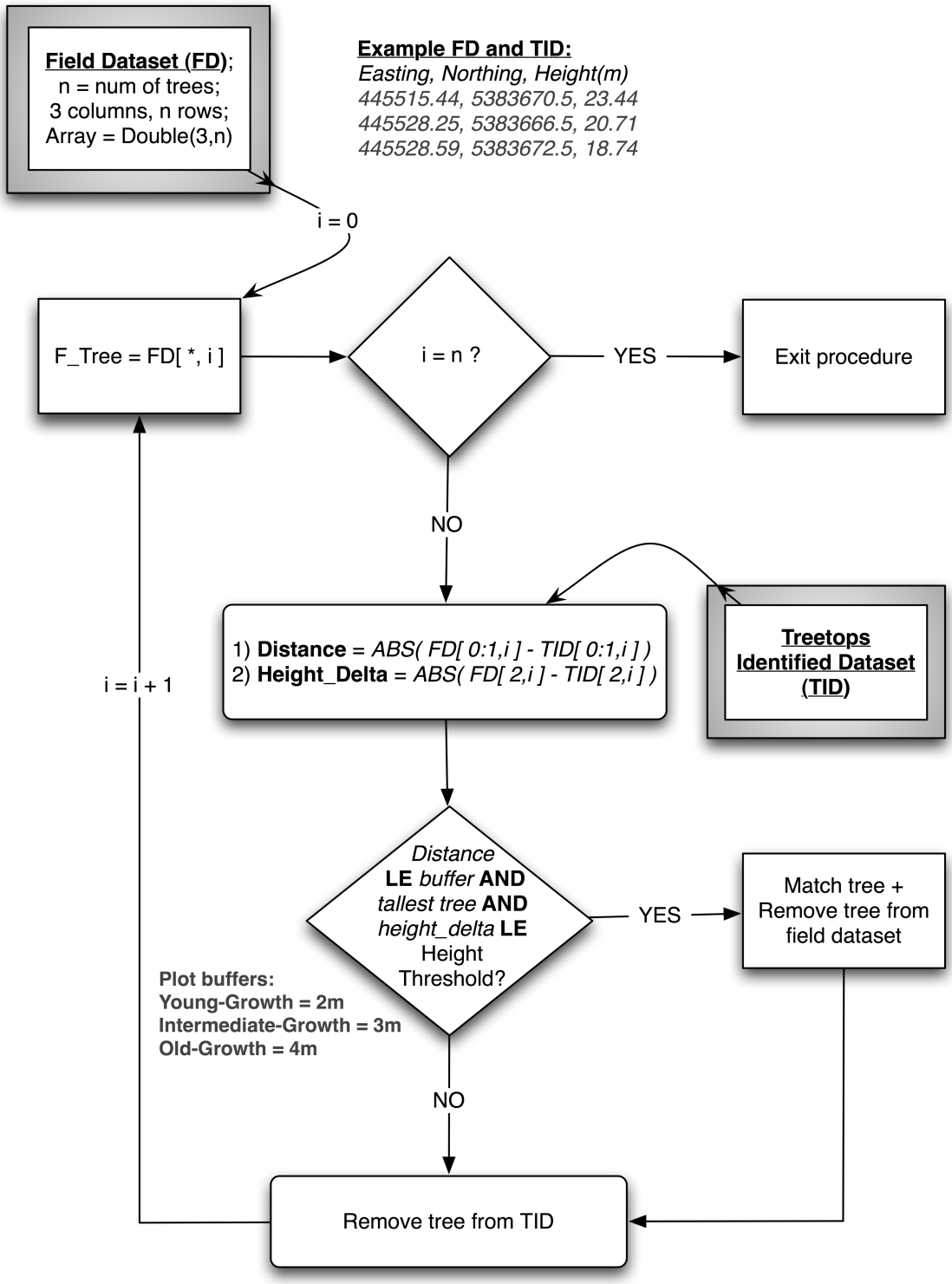


**Figure 21 - Treetop validation flowchart.**

## 5.4 - Partial crown delineation

Another aspect of crown delineation that is currently being explored is the identification and delineation of partial crowns corresponding to intermediate or suppressed trees located underneath the dominant/co-dominant canopy. This section presents preliminary methods used to identify the partial canopies, and explores some exciting new possibilities to better understand the vertical forest structure. The module is an exploratory tool that searches for new possibilities to improve and enhance, for example, the identification of ladder fuel underneath the dominant layer of vegetation in forested areas.

Using LiDAR raw points, this method assumed that it was possible to identify and locate a separation among vegetation layers in a forested area. There are two main important layers in a forested system, they are: height to living crown (HLC), and the top of suppressed canopy level (TSCL). The HLC was usually collected in the field, but not used in this study. To acquire the HLC it was necessary to understand two parameters that explain its vertical location: location of tree base (at soil surface), and maximum tree crown radius location. The vertical distance between these two parameters represented the tree HLC. With this parameter, it was possible to distinguish where the most dominant layer of vegetation was located in a vertical profile.

The focus of this module was the identification of trees below TSCL, which could behave as a fuel ladder in the study plots. For identifying this layer of vegetation it was important to understand where an abrupt change in density was located: the top of suppressed canopy level. The algorithm had to be able in recognizing these different layers of

vegetation and mark where the most discrepant change was located. This method was meant to be totally independent of field measurements, which was different from the HLC measurements that were usually collected in the field (figure 22). Also, not every single tree in a forested system was measured for HLC; this would be nearly impossible to accomplish especially when there are millions of trees. These data were then used to predict the HLC for study plots using a statistical model created from the acquired data. As shown in figure 22, the predicted HLC was observed around the maximum tree crown radii located in a study plot, while the TSCL represented the most abrupt change among the different vegetation layers in a plot. There are cases, where the HLC and the TSCL are at the same height. Assuming that a tree canopy started at the treetop height, points below the TSCL would represent the points used to identify partial crowns. As stated before, these points will represent vegetation underneath the dominant/co-dominant layer of vegetation, also representing the potential fuel ladder in a forest system.

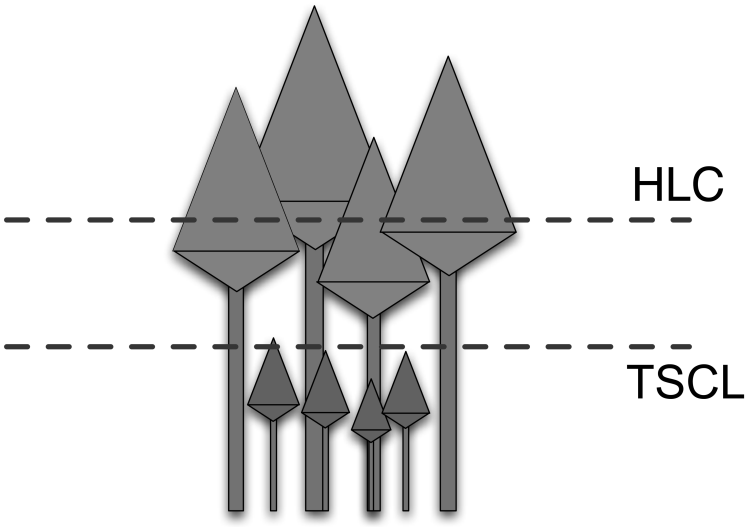


**Figure 22 - Comparison between Height to Living Crown (HLC) and the top of suppressed canopy level (TSCL).**

The identification of the TSCL started with the creation of two curves. The first curve represented the height percentiles, and the second curve represented the first derivative of the first curve. An abrupt change in curvature was expected in these curves, demonstrating the change in vegetation density (Figure 23).

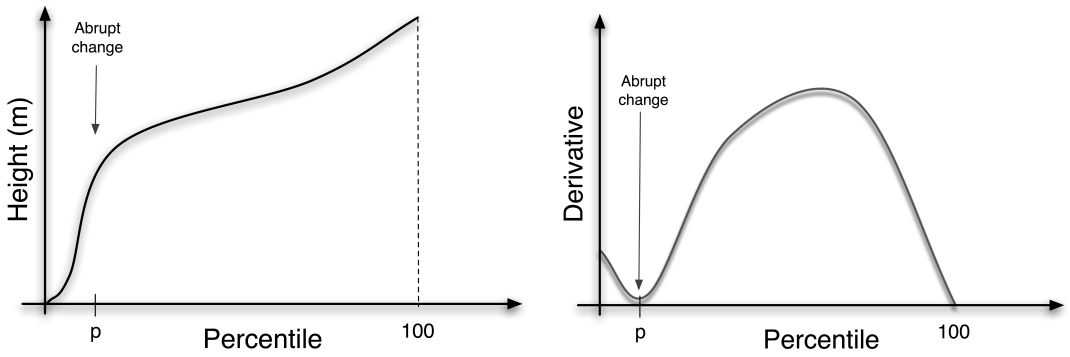


**Figure 23 – Simulated percentile and derivative curves showing the location of the abrupt change in curvature.**

The change should be at the same height percentile when comparing both curves, and it was expected to occur because of the dense dominant vegetation cover that reduces the amount of light dispersed throughout the canopies. This reduced amount of light was expected to affect the growth of the vegetation underneath this dominant layer, creating distinguishable vegetation layers with different densities. With the points below the TSCL in hand, the partial canopy identification was conducted. This process worked similarly to the treetop identification and dominant/co-dominant canopy delineation algorithms, where the highest point among all the points below the TSCL was located first. From that point, 36 iterations were conducted in order to locate the crown edges. These edges were then used as vertices to create a polygon to delineate the tree crown.

With the polygon identified it was then possible to remove all the LiDAR points that fell within this shape. With these points removed, it was possible for the algorithm to identify the next highest point in the dataset. The algorithm would then perform the same steps until all points were accounted for. To better understand the partial canopy process, a flowchart is presented in figure 24.

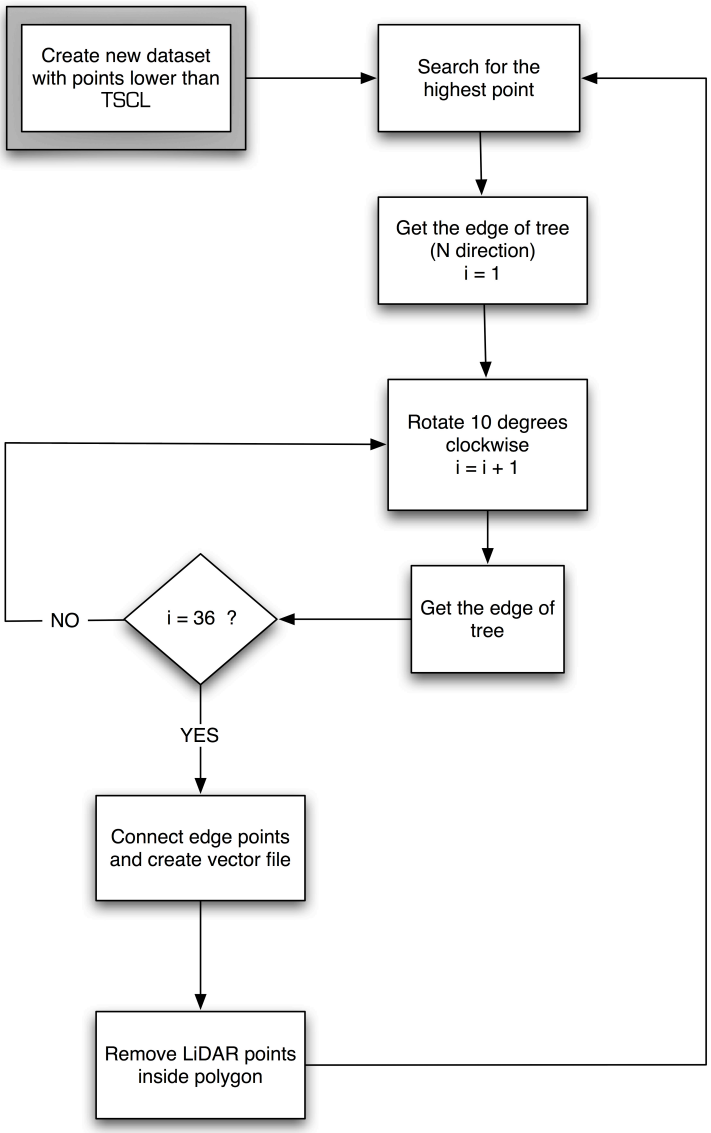


**Figure 24 - Partial canopy delineation flowchart.**

# Chapter 6: Results

The following chapter presents the results of the individual treetop identification, crown delineation, and partial crown delineation. The method described in section 5.3 was used to validate the identified treetop locations against surveyed field data. To visually demonstrate the results, LiDAR CHM images were used as background and results overlaid on the image.

## 6.1 – Individual treetop identification

The results for each identified treetop were simple coordinates containing one easting and one northing UTM location. Also, the height of the identified tree in metres was assigned to each treetop. To better illustrate the treetop locations in the study area, LiDAR background images were used and results overlaid on them. In addition, convex hulls of the surveyed trees in the field were used to delineate the plot boundaries. Figure 25 presents the plot boundaries (shown as red polylines), the identified treetops positions (shown as blue dots), and matched identified treetops with field data (shown as red squares).

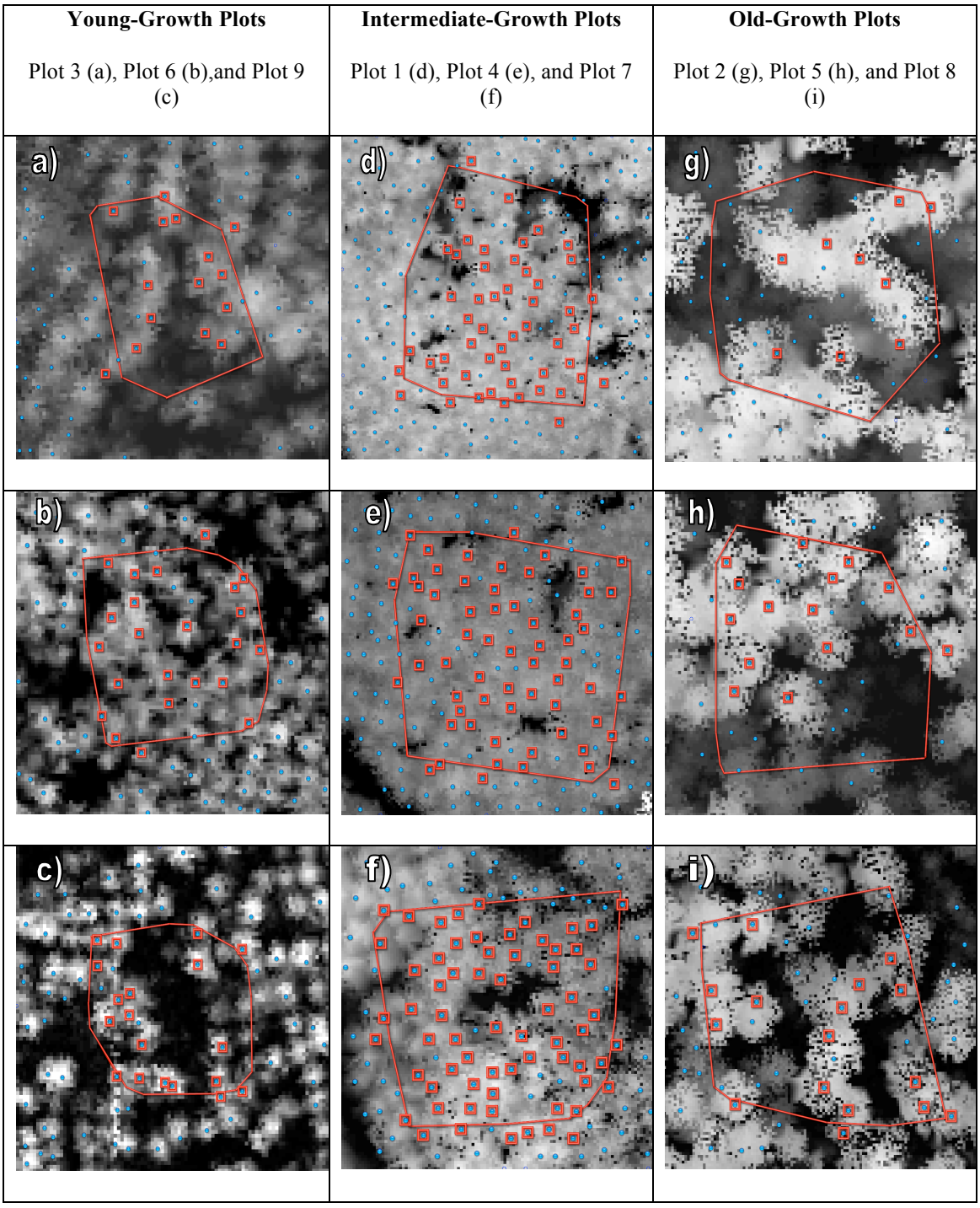


**Figure 25 - LiDAR CHM data as background, treetops represented as blue dots and plot boundary as red polyline. Red squares represent tree locations matched with field data.**

The individual treetop algorithm was able to identify more than 79% of all dominant and co-dominant trees in the nine surveyed plots. The following paragraphs will present more details of the results for each plot surveyed in the field. The results of "matched" trees, presented in this section, represent the percentage of trees that had similar coordinates and heights, when comparing algorithm outputs and field data. This percentage is related only to dominant and co-dominant trees surveyed in the field.

Young-growth plots presented the lowest percentage in "matched" trees. For plot 3, 20 "dominant" and "co-dominant" trees were surveyed in the field. Using the validation method, 15 trees were matched with the field data (red squares, Figure 25a), totaling 75% of "dominant" and "co-dominant" trees. The average displacement of the easting UTM coordinate was ± 1.1 m, and ± 1.3 m for the northing UTM coordinate. For plot 6, 34 "dominant" and "co-dominant" trees were surveyed in the field, where 23 trees were matched with field data, totaling 68% of the trees identified. The average displacement for this plot was ± 1.3 m for the easting UTM coordinate and ± 1.8 m for the northing UTM coordinate. Finally, plot 9 had 26 "dominant" and "co-dominant" trees surveyed in the field, with 19 trees matched, or 73% of identified trees. Plot 9 presented the lowest displacement among young-growth plots with ± 1.0 m for the easting UTM coordinate and ± 0.7 m for the northing UTM coordinate.

The LiDAR background images helped provide a better understanding of how dense the forest cover was. This was possible by observing the pixel brightness, where a homogeneous brightness within the study area represented constant tree heights. On the

other hand, heterogeneous brightness indicateed the presence of varied tree heights and/or gaps within the study area. Intermediate-growth plots usually had homogeneous heights, presenting similar brightness pixels within the study area (Figure 25 (d-f)).

As for the results of intermediate-growth plots, the algorithm was able to identify more than 83% of the "dominant" and "co-dominant" treetops. Plot 1 presented the highest percentage (88%) of identified trees, where 52 out of 59 trees were matched. The average displacement was ± 1.6 m for the easting UTM coordinate and ± 1.5 m for the northing UTM coordinate. For plot 4, 71 "dominant" and "co-dominant" trees were surveyed in the field, where 61 trees were matched with the field data, totaling 86% of "dominant" and "co-dominant" trees. The average displacement for this plot was ±1.6 m for the easting UTM coordinate and ±1.7 m for the northing UTM coordinate. The last intermediate-growth plot, plot 7, presented 87 "dominant" and "co-dominant" trees surveyed in the field, with 66 trees matched with the field data, a total of 76% of "dominant" and "co-dominant" trees. The average displacement of plot 7 was ±1.4 m for the easting UTM coordinate and ±1.8 m for the northing UTM coordinate.

Old-growth plots were quite different from intermediate-growth plots. Old-growth plots presented an increased amount of gap area and different tree heights within plots, easily observed by the heterogeneous pixel brightness on Figures 25 (g-i). The algorithm was also able to find the majority of the "dominant" and "co-dominant" trees, with an average greater than 82% of identified treetops. The first old-growth plot, plot 2, had 12 "dominant" and "co-dominant" trees surveyed in the field. From these 12 surveyed trees,

9 trees were successfully matched, totalling 75% of identified treetops. The average displacement was ±1.4 m for the easting UTM coordinate and ±1.5 m for the northing UTM coordinate. Plot 5 had the highest percentage of identified treetops among old-growth plots. 15 trees out of 17 surveyed in the field were matched, totalling 88% of identified trees. The average displacement for the easting and northing UTM coordinate was ±1.7 m and ±0.8 m respectively. Finally, plot 8 had 20 "dominant" and "co-dominant" trees surveyed in the field, where 17 of these were successfully matched. The total percentage of identified treetops was 85%, and the average displacement was ±1.0 m for the easting UTM coordinate and ±1.4 m for the northing UTM coordinate.

Figure 26 and table 5 provide a summary of the results for all surveyed plots. The "Identified" column represents the "dominant" and "co-dominant" trees identified by the algorithm, while column "Surveyed" represents the "dominant" and "co-dominant" trees surveyed in the field. The average displacement based on the easting and northing UTM coordinates is also provided in this table with the respective standard deviation (S.D.).

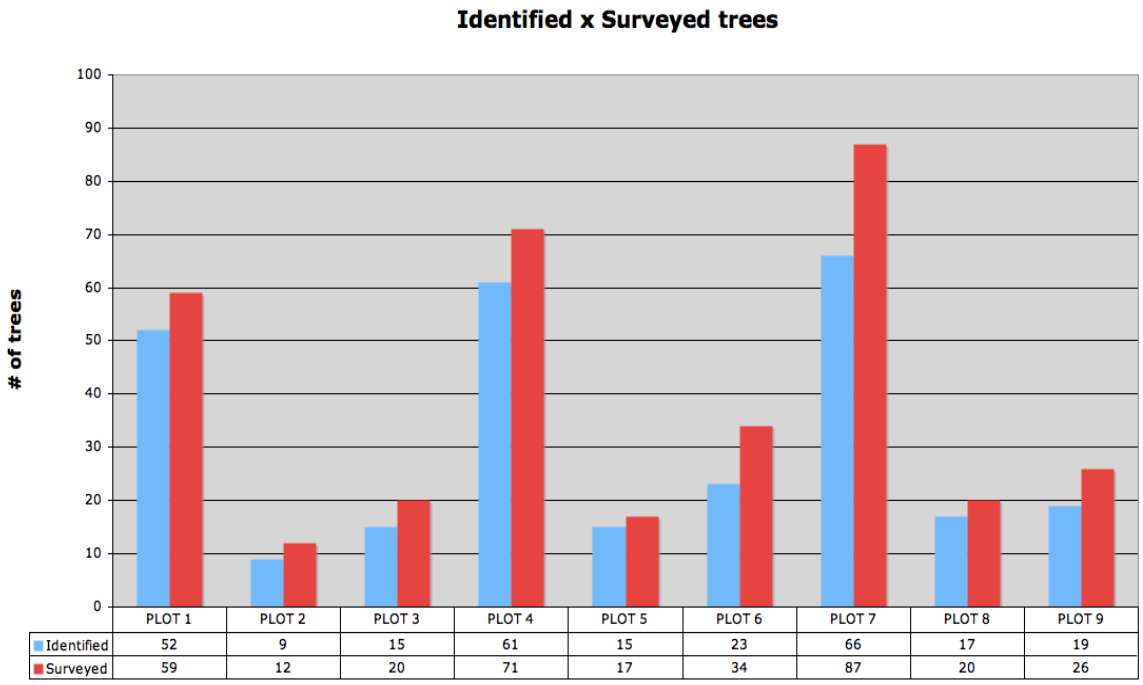


**Figure 26 - Results of identified and surveyed trees per plot.**

**Table 5 - Summary of all surveyed plots.**

| PLOT | % Identified | Average Disp. Easting | Average Disp. Northing |
|---|---|---|---|
| 1 | 88 | ±1.4 m; *S.D.=1.11* | ±1.2 m; *S.D.=1.18* |
| 2 | 75 | ±1.5 m; *S.D.=1.35* | ±1.5 m; *S.D.=1.07* |
| 3 | 75 | ±1.2 m; *S.D.=0.82* | ±1.0 m; *S.D.=0.98* |
| 4 | 86 | ±1.3 m; *S.D.=0.87* | ±1.6 m; *S.D.=1.19* |
| 5 | 88 | ±1.6 m; *S.D.=0.79* | ±1.3 m; *S.D.=1.65* |
| 6 | 68 | ±0.8 m; *S.D.=0.71* | ±1.4 m; *S.D.=1.12* |
| 7 | 76 | ±1.4 m; *S.D.=1.17* | ±1.7 m; *S.D.=1.11* |
| 8 | 85 | ±1.2 m; *S.D.=0.84* | ±1.3 m; *S.D.=1.07* |
| 9 | 73 | ±0.9 m; *S.D.=0.42* | ±0.6 m; *S.D.=0.30* |

## 6.2 – Crown delineation

This section is intended to give some insight into the canopy delineation results (Figures 27 (a-j)). Again, LiDAR images were created from the CHM data and used as background to help visualize the location of the identified treetops.

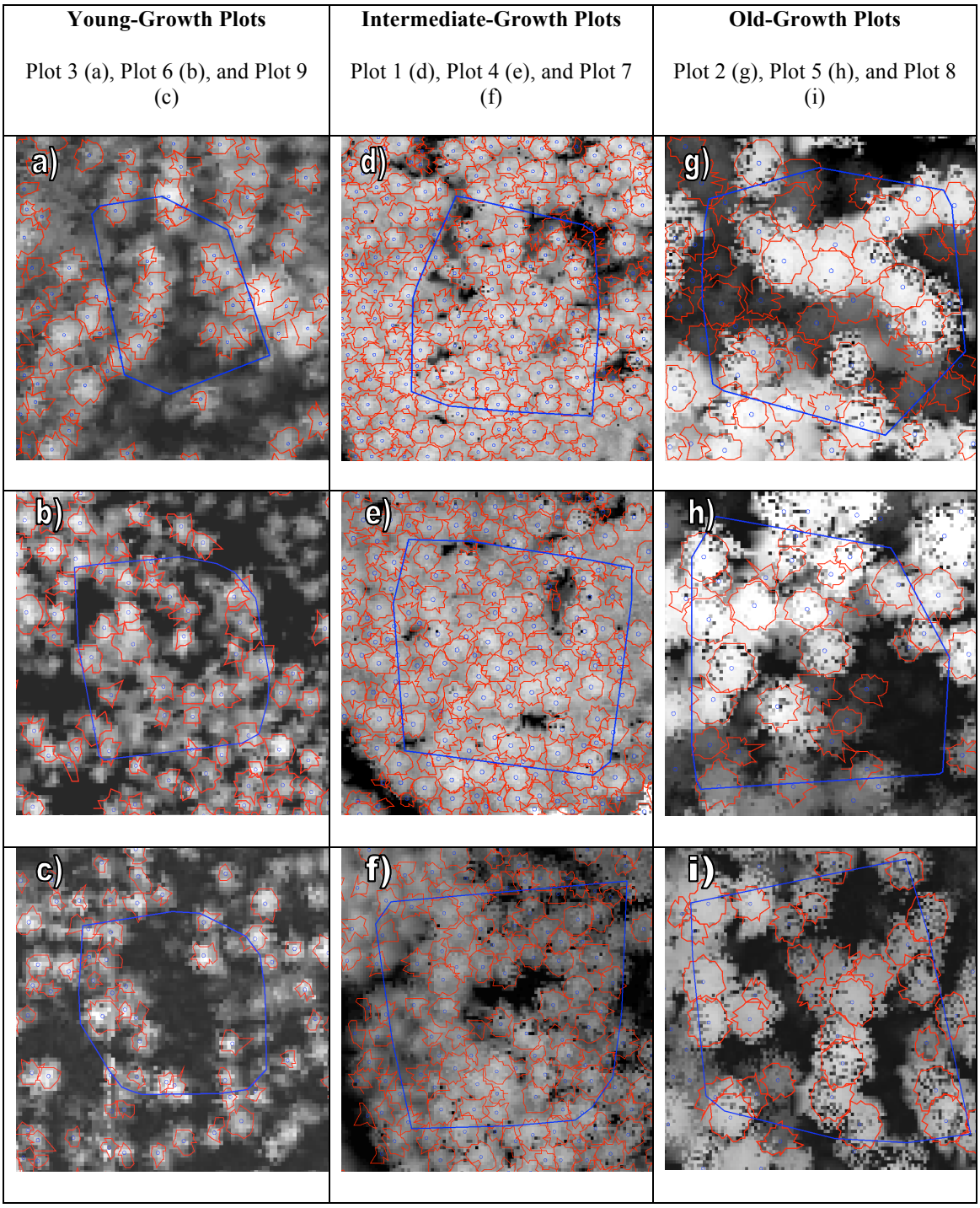


**Figure 27 - LiDAR CHM data as background, treetops represented as blue dots and plot boundary as blue polyline. Red polygons represent delineated crowns.**

The algorithm performed well in delineating tree crowns, especially for intermediate and old-growth plots. Young-growth plots presented a more challenging scenario for the algorithm. Within these plots, trees were not taller than 17 m (section 5.2), and canopy interaction was commonly seen (Figure 4a). Lower vegetation was present underneath the dominant layer in young-growth plots, easily seen on the LiDAR images (Figure 27 (a-c)) and on photos taken in the field (Figures 4 (a-c)). Despite the challenge, the algorithm was able to delineate the dominant tree crowns for these young-growth plots. For plot 3, the average delineated radius was 1.54 m against the 2.57 m measured in the field; Plot 6 presented average identified radius of 1.50 m against 1.98 m measured in the field; and plot 9, among the young-growth plots, presented the smallest difference between delineated and measured radii, with average of 1.58 m against 1.88 m respectively.

Intermediate-growth plots presented similar heights within plots. It was possible to observe that when examining the LiDAR raster images used as background in this section (Figure 27 (d-f)). There was not much difference in brightness among the tree raster images, thus showing the close to constant heights within each plot. With this homogeneous dominant layer of vegetation it was not possible to clearly distinguish crown edges, and illustrated a scenario of intense interaction between tree canopies. Even so, the algorithm performed well in delineating the crowns around the previously identified treetops, with average delineated radius for plot 1 of 1.99 m against 2.44 m measured in the field; average identified radius of 1.96 m against 2.74 m measured in the field for plot 4; and average identified radius of 1.90 m against 2.79 m measured in the field.

Old-growth plots were usually composed of two major layers of vegetation. The primary layer represented the dominant and co-dominant trees in the area, and the secondary layer represented trees and shrubs underneath the primary layer. This was possible to observe on the LiDAR background images displayed in this section (Figures 27 (g-i)). The algorithm had no problems in delineating the dominant and co-dominant trees crowns for the previous identified treetops. Also, the algorithm was able to delineate trees underneath the dominant layer of vegetation visible through gaps. For plot 2, the average radius identified by the algorithm was 2.89 m against 2.99 m measured in the field. Plot 5 presented a more intense interaction of old-growth trees compared to plot 2. Even so, the algorithm performed well in delineating the crowns resulting in an identified average radius of 2.87 m against 3.72 m measured in the field. Plot 8 presented a more homogeneous cover of old-growth trees (Figure 27i), where not much vegetation is seen through the existing gaps. For plot 8 an average radius of 2.75 m was identified against 2.82 m measured in the field.

Figure 28 provides a summary of the average radii measured in the field and the ones obtained by the algorithm delineation of crowns.

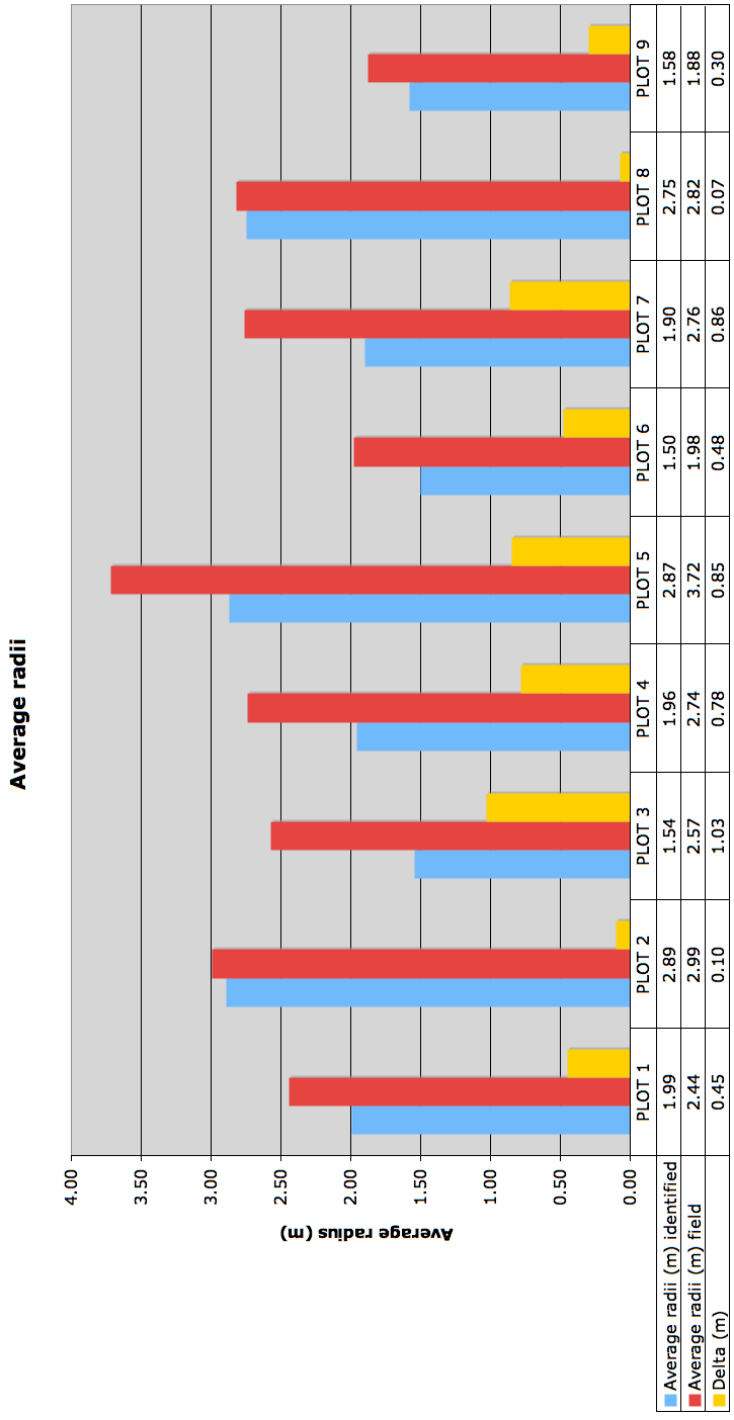


**Figure 28 - Results of average radii of crowns measured in the field and outlined by the algorithm.**

In summary, the algorithm performed well in delineating tree crowns, especially for intermediate and old-growth plots. Dense plots like the intermediate-growth plots were not a problem for the algorithm, and it was able to delineate crowns even with intense interaction among canopies. The different layers of vegetation observed in the old-growth plots were also not a problem for the success of crown delineation. The algorithm was able to delineate crowns within these different layers when visible through gaps.

### 6.3 - Partial crown delineation

This section will provide the results acquired for the partial tree crown delineation. Figures 29 and 34 present percentiles and derivatives to predict TSCL. For each plot, charts with height percentiles and respective derivatives will be presented first. Based on the predicted TSCL value the following figures will present the LiDAR points that are above and below the predicted TSCL.

#### 6.3.1 – Intermediate-growth plots

Figure 29 provided a graphical representation of TSCL for the intermediate-growth plots. For each plot, charts were created representing two different curves. The first curve was created based on tree heights against their corresponding percentile, and the second curve represented the percentile's derivative curve. The percentile curves indicated where a break, or discrepancy, in height existed when examining the height of vegetation layers. In the derivative curve, this break was located at its minimum point. This minimum

represented the height percentile that could be easily converted to the actual height in metres. This value was marked in red on every derivate curve in Figure 29.

Examining the derivative curve for plot 1 (Figure 29a), it was evident that the curve reached its minimum just before the 15$^{th}$ percentile, representing a height of 9.35 m. Plot 4 presented a more interesting scenario compared to the previous plot. Both plots were categorized as intermediate-growth plots, but plot 4 had a lower TSCL value than plot 1. The minimum value for the derivative curve was observed on the 5$^{th}$ percentile, representing a height of 4.74 m (Figure 29b). Plot 7 had the lowest TSCL value among the intermediate-growth plots. The minimum value for the derivative curve was reached at the 10$^{th}$ percentile, representing the small height of 1.69 m (Figure 29c).

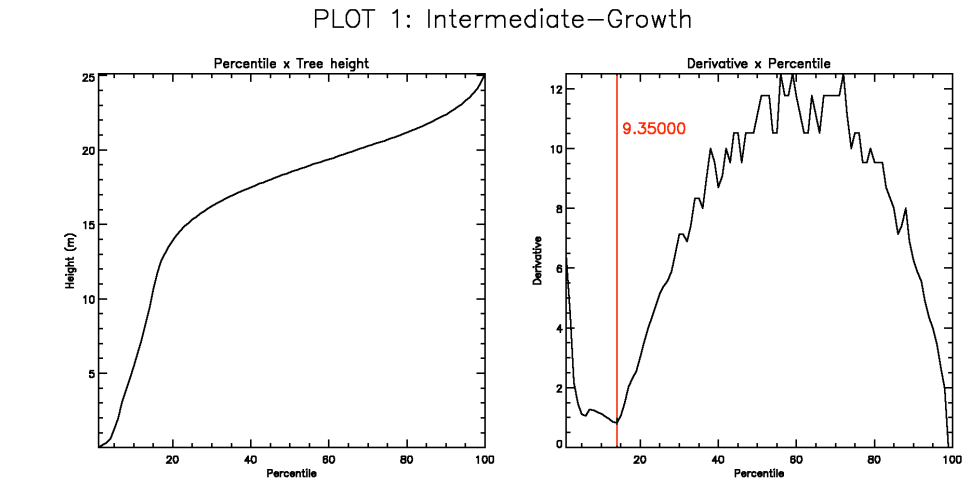


**a)**

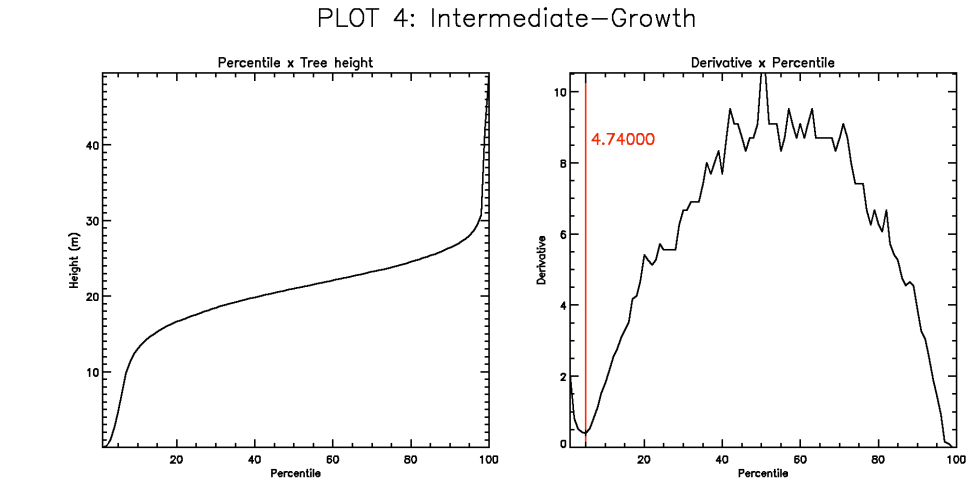


**(b)**

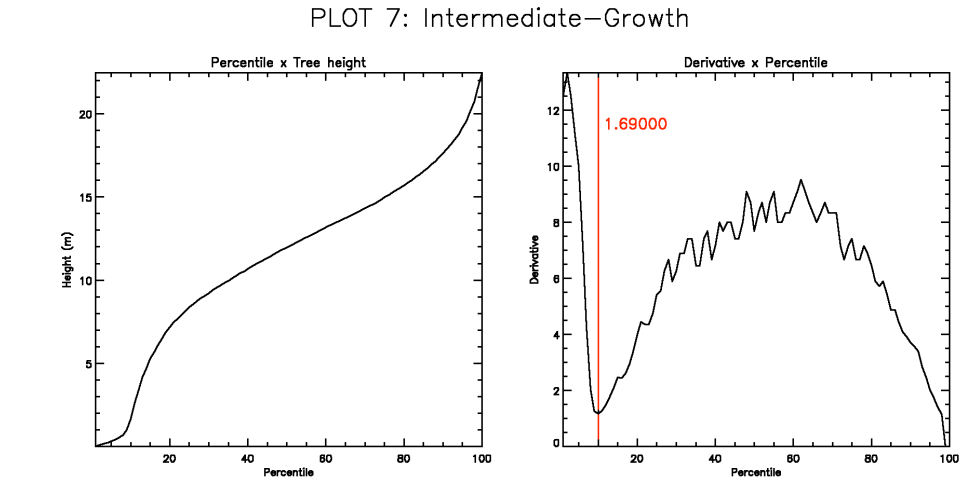


**c)**

**Figure 29 - Chart containing percentile and derivative curves for intermediate-growth plots. Red line indicates TSCL in metres.**

The next figures (Figures 30-32) provided a better understanding of how the derivative curves helped in differentiating the distinct layers of vegetation in the study plots. Using TSCL as a threshold it was possible to separate the two main layers of vegetation (dominant trees and vegetation underneath dominant trees) based on LiDAR points. The dominant trees were represented as green dots, and trees underneath this dominant layer as brown dots. The identification of partial canopies could take place only after the LiDAR points underneath the TSCL threshold was selected. Using the method described in section 5.4 it was then possible to obtain the results in figures 30-32, where the identified treetops of the partial canopies were displayed over LiDAR points (blue dots). The blue polygons represented plot boundaries created from surveyed tree locations.

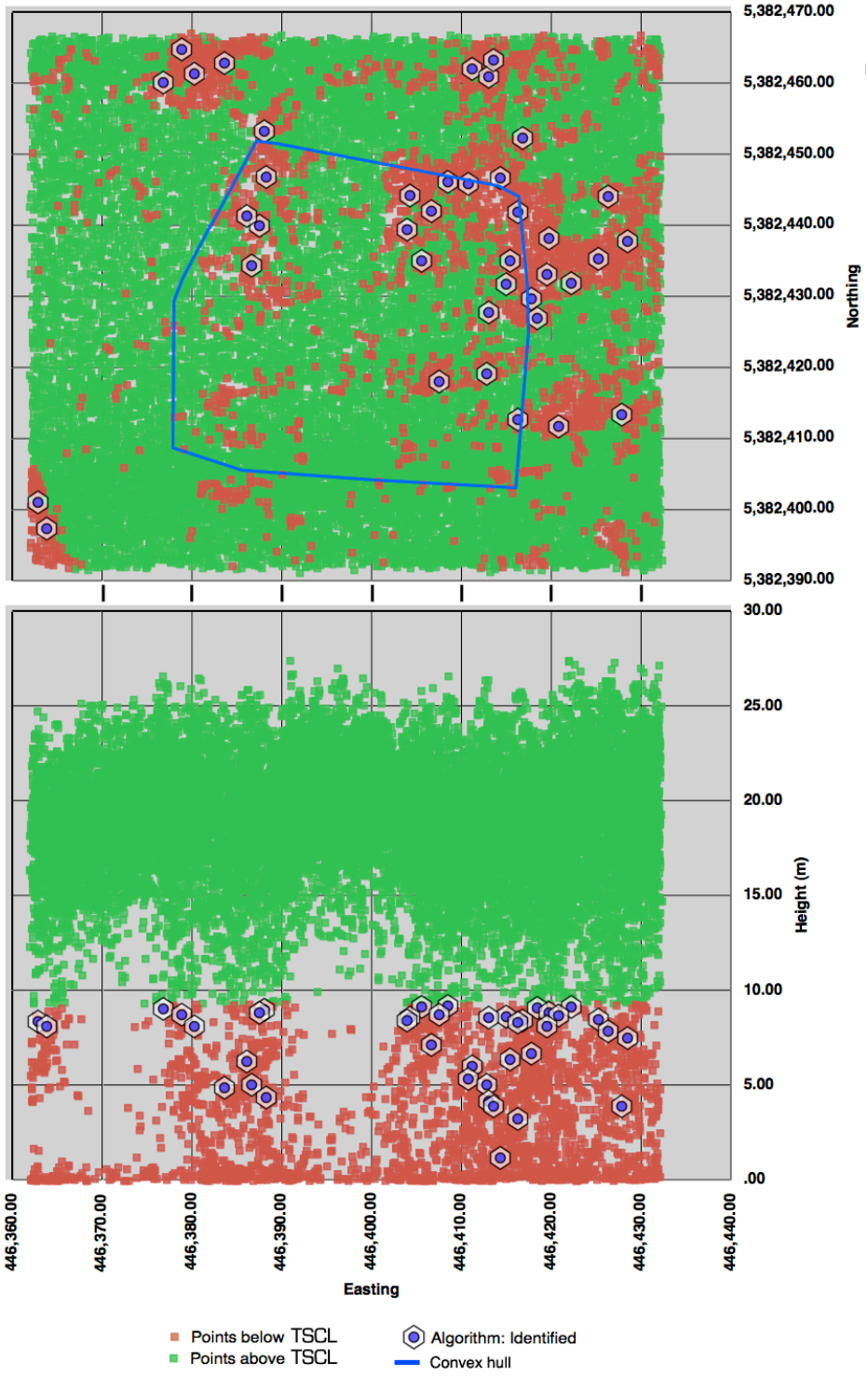


**Figure 30 - Top figure shows a plan-view of plot 1, and bottom figure a vertical profile for the same plot. Green dots represent dominant trees; brown dots represent trees underneath dominant layer.**

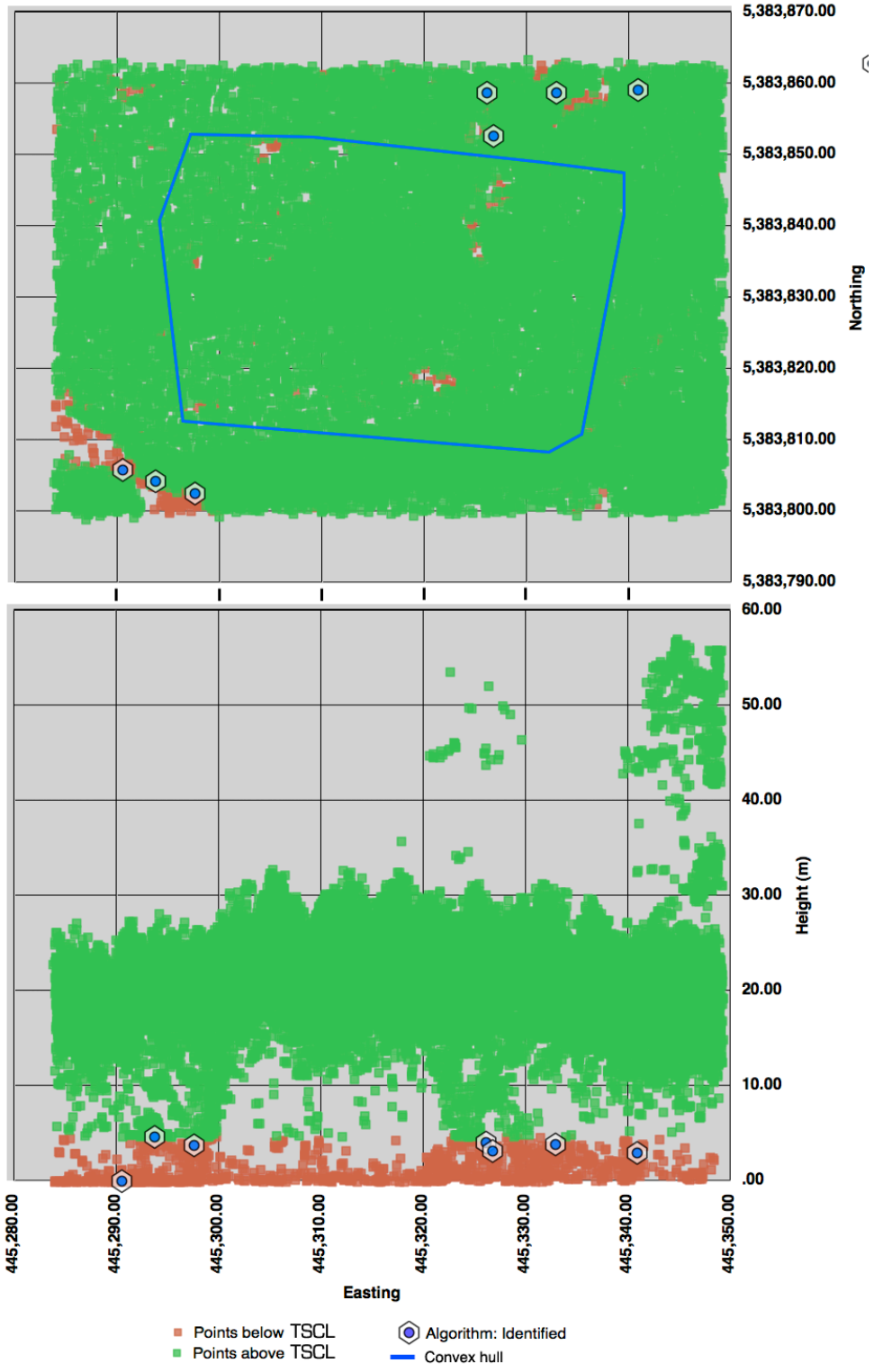


**Figure 31 - Top figure shows a plan-view of plot 4, and bottom figure a vertical profile for the same plot. Green dots represent dominant trees; brown dots represent trees underneath dominant layer.**

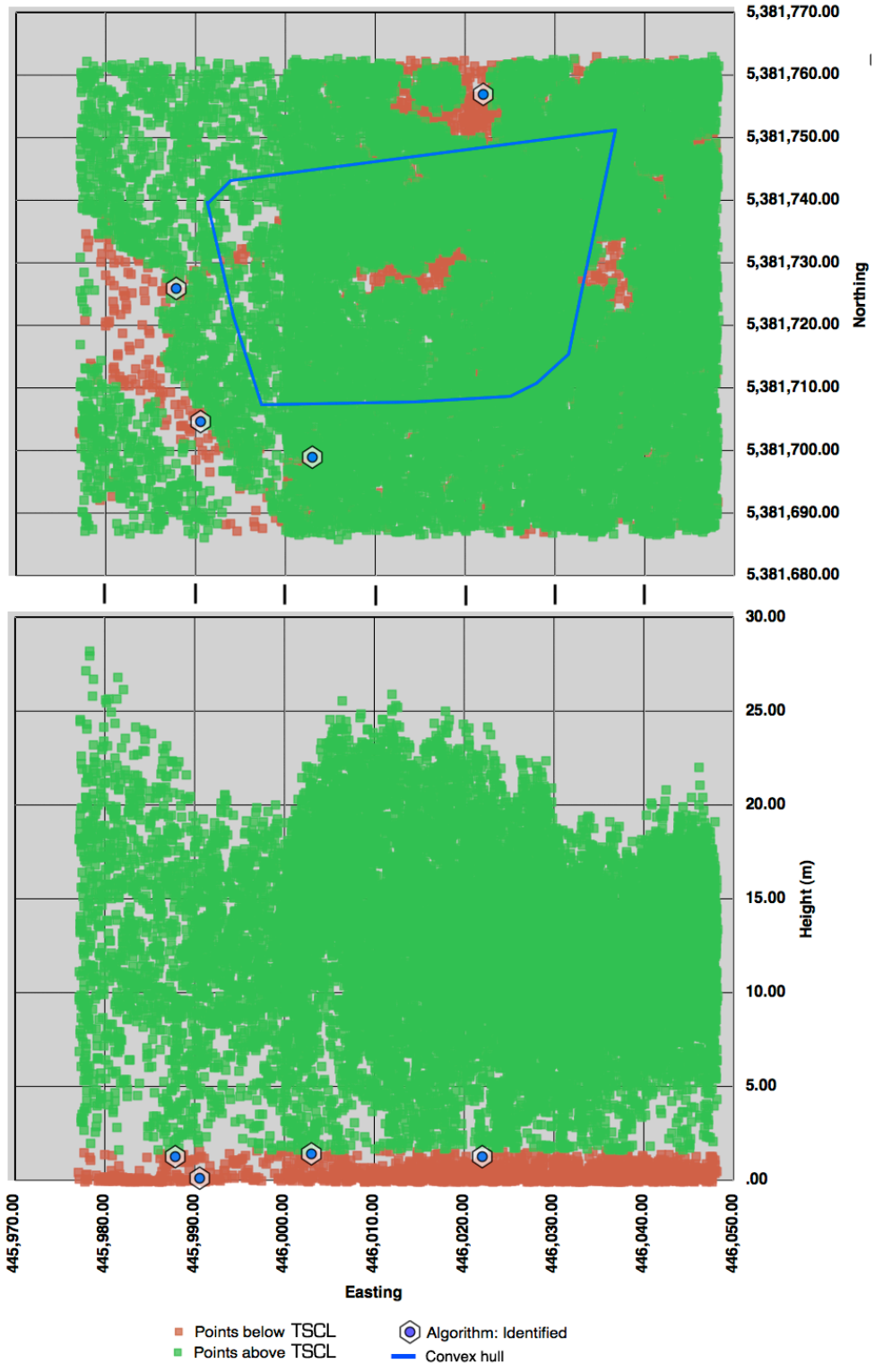


**Figure 32 - Top figure shows a plan-view of plot 7, and bottom figure a vertical profile for the same plot. Green dots represent dominant trees; brown dots represent trees underneath dominant layer.**

What was clearly noticeable in the intermediate plots was the dense dominant layer of vegetation. Also, the majority of intermediate trees were mixed in this dominant layer (yellow dots in figures 30-32). For plot 1, the number of intermediate trees was 110. The algorithm was able to identify 17 trees using the TSCL threshold method within the plot boundaries. Plot 4 presents a similar scenario, where a dense dominant layer of vegetation was easily identified when using the TSCL as threshold (Figure 31). Again, the intermediate trees were mixed in this dominant layer of vegetation, and no surveyed trees in the field were observed below the TSCL threshold value. The algorithm was not able to identify any of the 50 intermediate canopies surveyed in the field. The only identified canopies were outside the plot boundaries (Figure 31). Similarly to plot 4, plot 7 did not present many points below the TSCL threshold. Also, for this plot, the algorithm was not able to identify any canopy within the plot boundaries (Figure 32).

In summary, for the intermediate-growth plots the dense dominant layer of vegetation was easily observed, and not many LiDAR points close to the surface of the ground (Figure 33). It was also possible to verify the existence of patches of LiDAR points in the first metres close to the ground. This was observed only because of the presence of gaps in the dominant layer of vegetation.

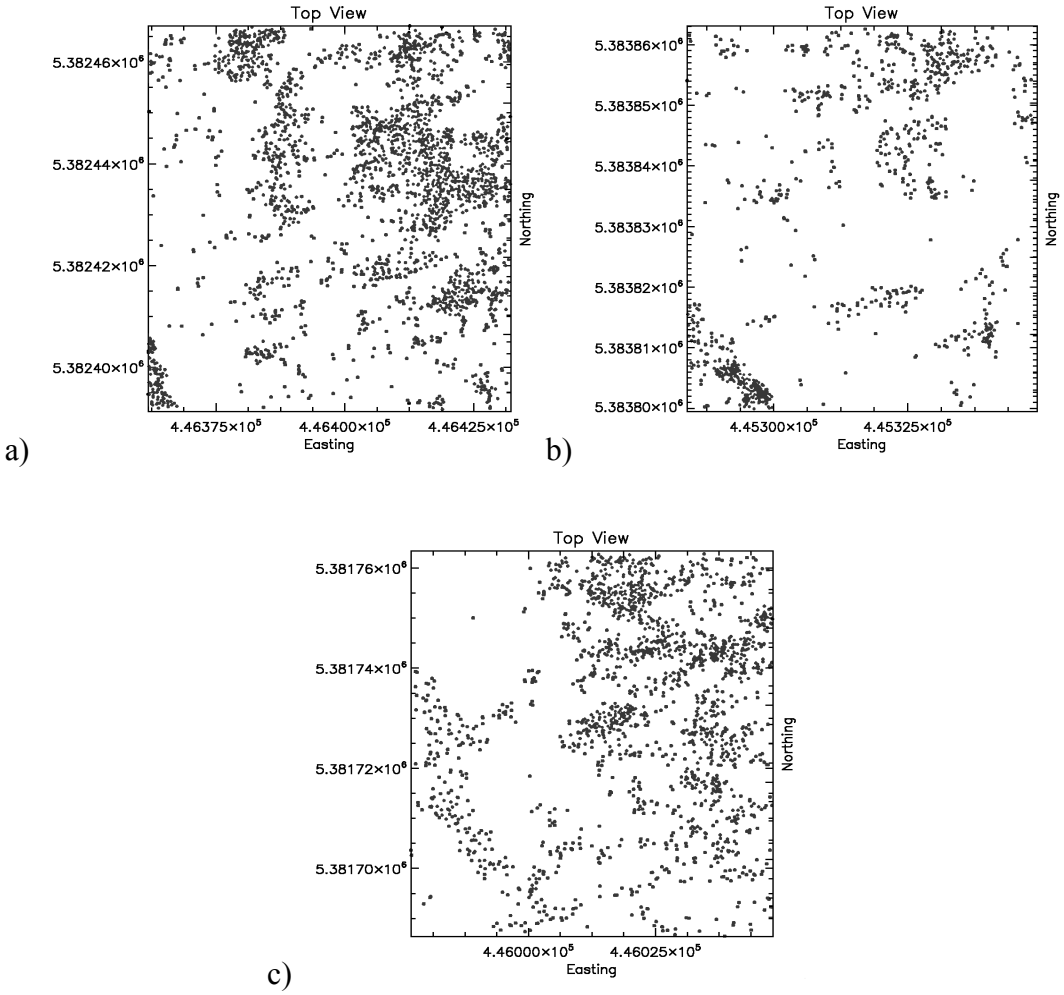


**Figure 33 - Plan-view of intermediate-growth plots showing LiDAR points below TSCL.**

### 6.3.2 – Old-growth plots

The same methods for acquiring TSCL heights were applied to the old-growth plots. The following figures present the threshold value found for each plot when observing the most imminent inflection point on the derivative curve. It was observed, on average, that old-growth plots return TSCL values higher than intermediate plots.

Plot 2 represented an old-growth plot, where trees reached more than 60 m in height (Figure 34a). The derivative curve reached its minimum just before the 45$^{th}$ percentile, representing the height of 27.73 metres (Figure 34a). Different from plot 2, plot 5 presented more points close to the ground surface. This was observed in figure 34b, where a distinct layer of LiDAR points was visible at the first metres from the ground surface. Also, it was not possible to observe a drastic change in curvature above the 20th percentile in plot 5 (Figure 34b). The derivative curve reacheed its minimum just above the 55$^{th}$ percentile, representing the height of 24.69 m (Figure 34b). Similar to plot 5, plot 8 presented many points close to the ground surface. This was also observed in figure 34c, where a distinct layer of LiDAR points was visible at the first metres from the ground surface. Also, it was not possible to observe a drastic change in curvature above the 20$^{th}$ percentile in plot 5 (Figure 34c). The derivative curve reacheed its minimum just above the 25$^{th}$ percentile, representing the height of 7.68 m (Figure 34c).

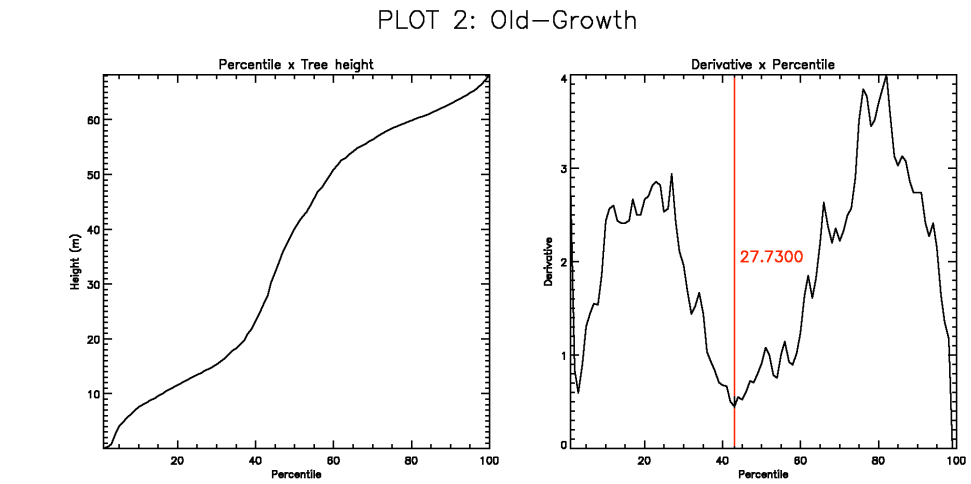


**(a)**

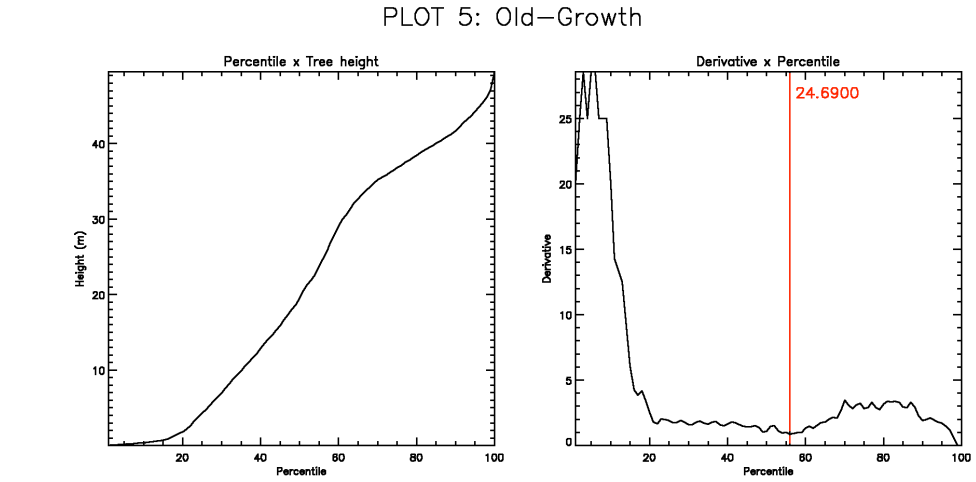


**(b)**

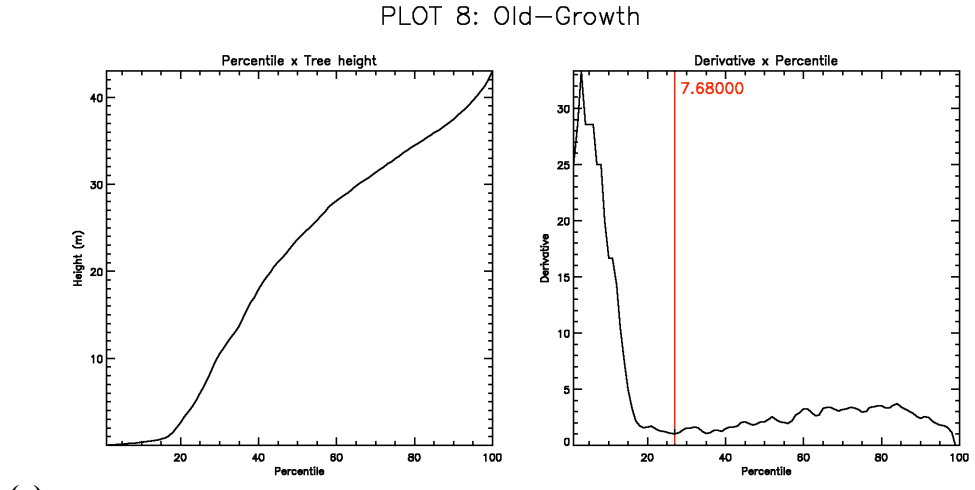


**(c)**

**Figure 34 - Chart containing percentile and derivative curves for old-growth plots. Red line indicates TSCL in metres.**

After obtaining the TSCL threshold it was then possible to separate the LiDAR points into two distinct classes. These were the same classes created for the intermediate-growth plots, and they represented the dominant layer of vegetation (represented as green dots in figures 35-37), and vegetation underneath these dominant layer (represented as brown dots).

It was possible to observe a more distinguished break between layers in plot 2 in figure 35. Clouds of LiDAR points concentrated more at the top and in the middle of the vertical profile. For this plot, the algorithm was able to identify 23 trees using the TSCL threshold. Plots 5 and 8 presented a thicker layer of smaller trees compared to plot 2. This was possible to observe in figures 34b and 34c, where the percentile-height curve had a constant increase before the $20^{th}$ percentile. Also, there was not an intense change in vegetation layers above the $20^{th}$ percentile demonstrating a more intrinsic growth among intermediate and old trees in these two plots. This was supported by the lack of a significant inflection point on the derivative curve similar to the one observed in plot 2. As for the identified results, the algorithm was able to identify 10 out of 13 intermediate trees surveyed in the field within plot 5 (Figure 36). Finally, the algorithm was able to identify 18 out of 28 intermediate-growth trees surveyed in the field within plot 8 (Figure 37).

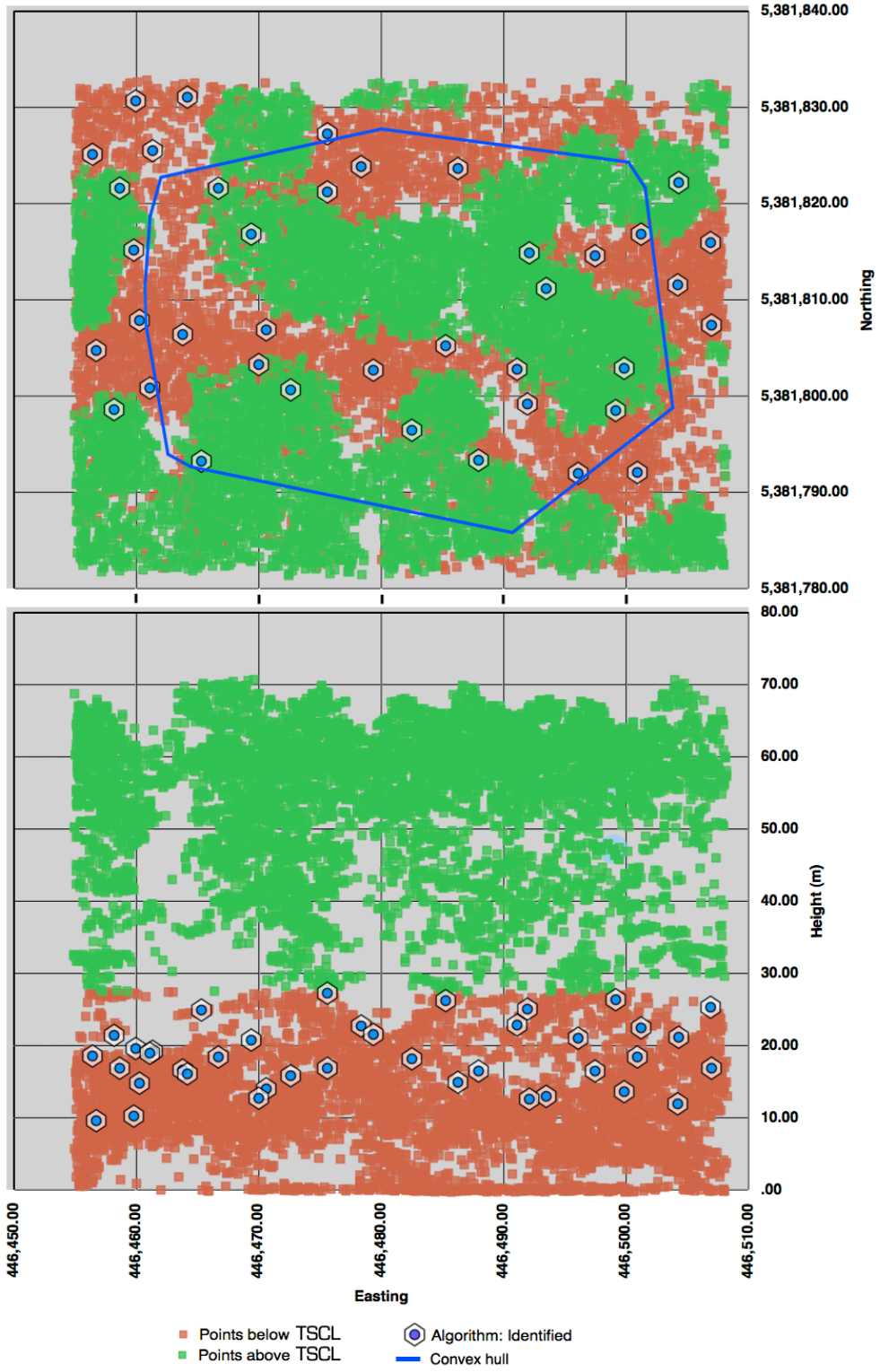


**Figure 35 - Top figure shows a plan-view of plot 2, and bottom figure a vertical profile for the same plot. Green dots represent dominant trees; brown dots represent trees underneath dominant layer.**

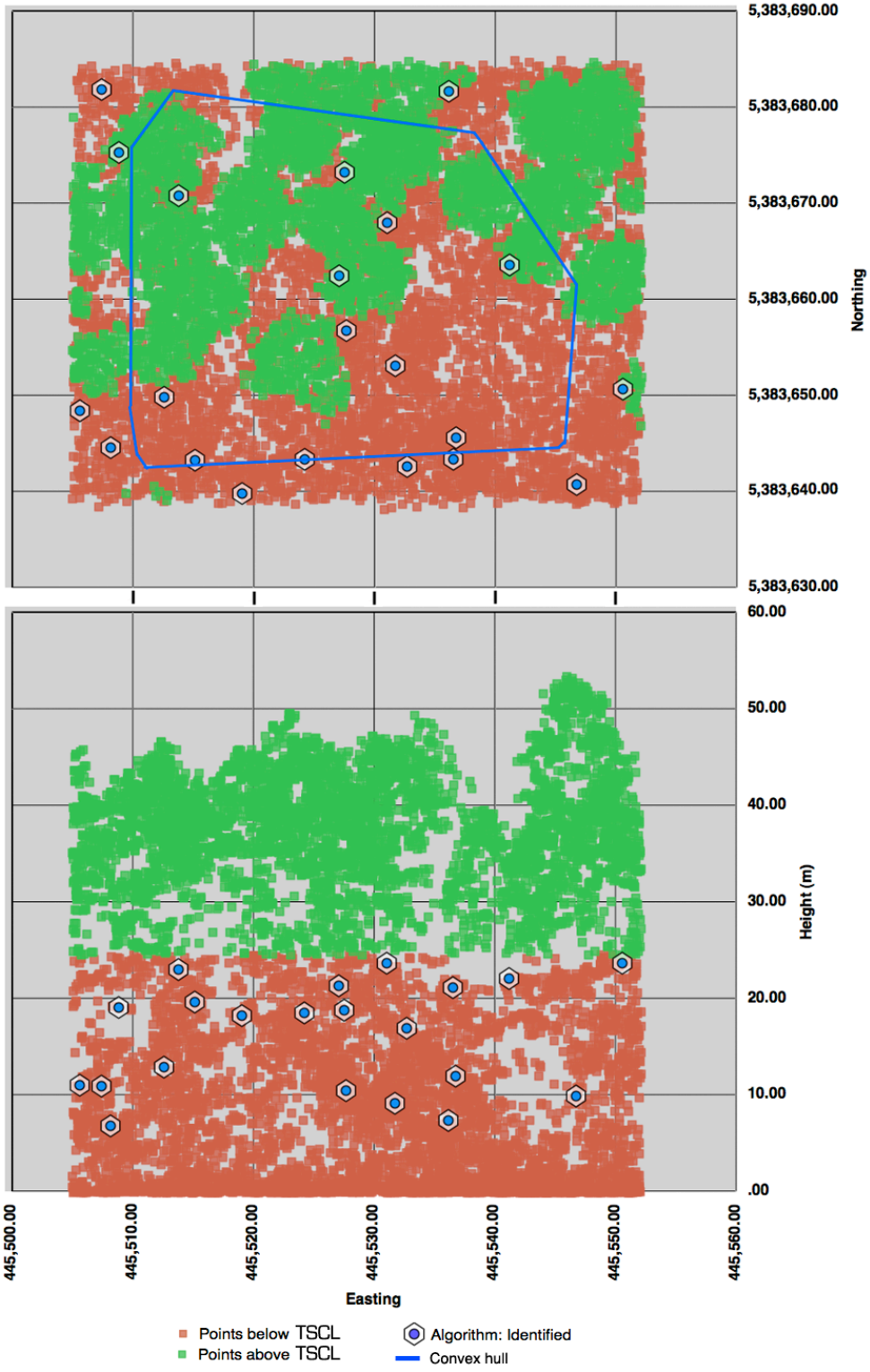


**Figure 36 - Top figure shows a plan-view of plot 5, and bottom figure a vertical profile for the same plot. Green dots represent dominant trees; brown dots represent trees underneath dominant layer.**

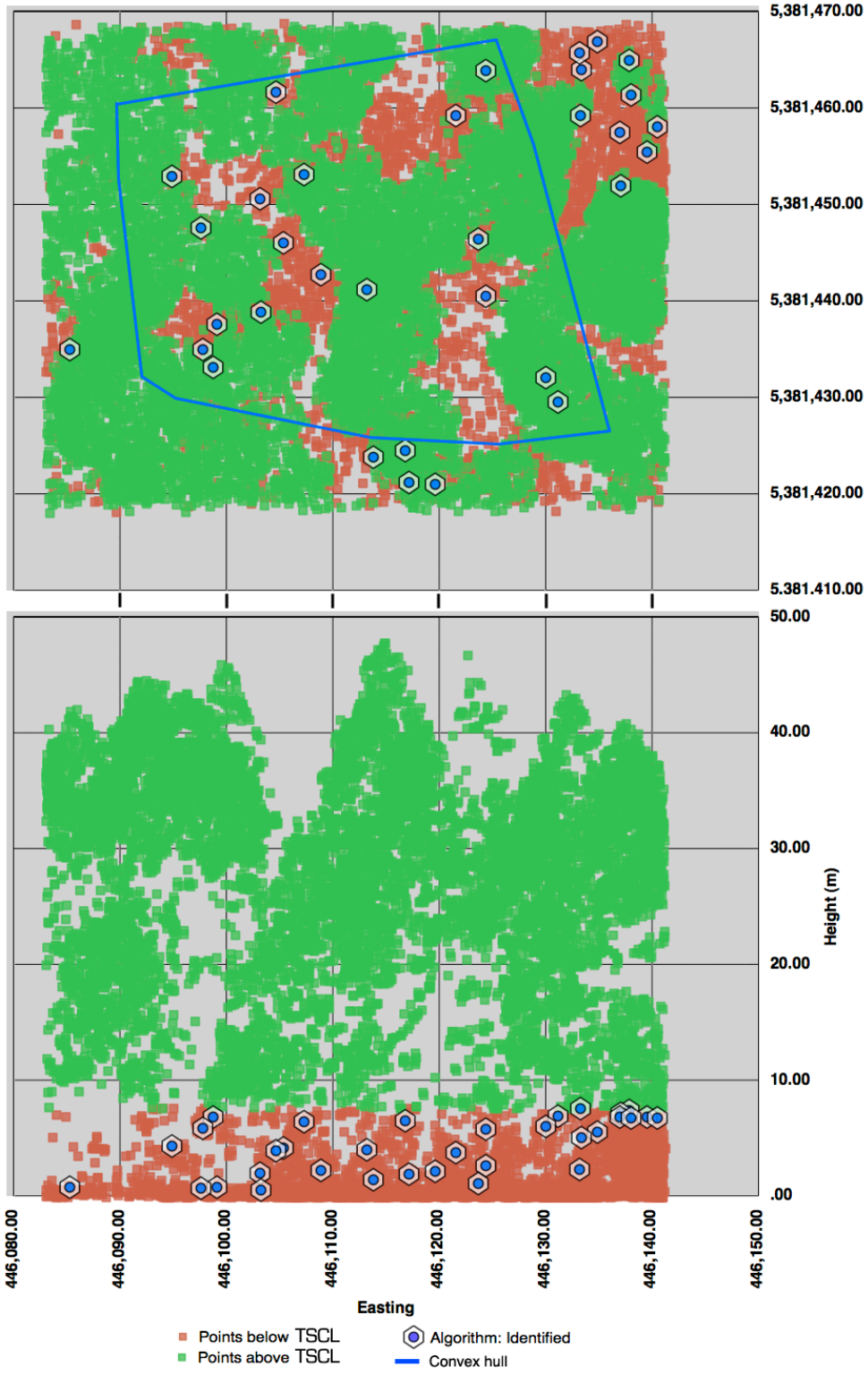


**Figure 37 - Top figure shows a plan-view of plot 8, and bottom figure a vertical profile for the same plot. Green dots represent dominant trees; brown dots represent trees underneath dominant layer.**

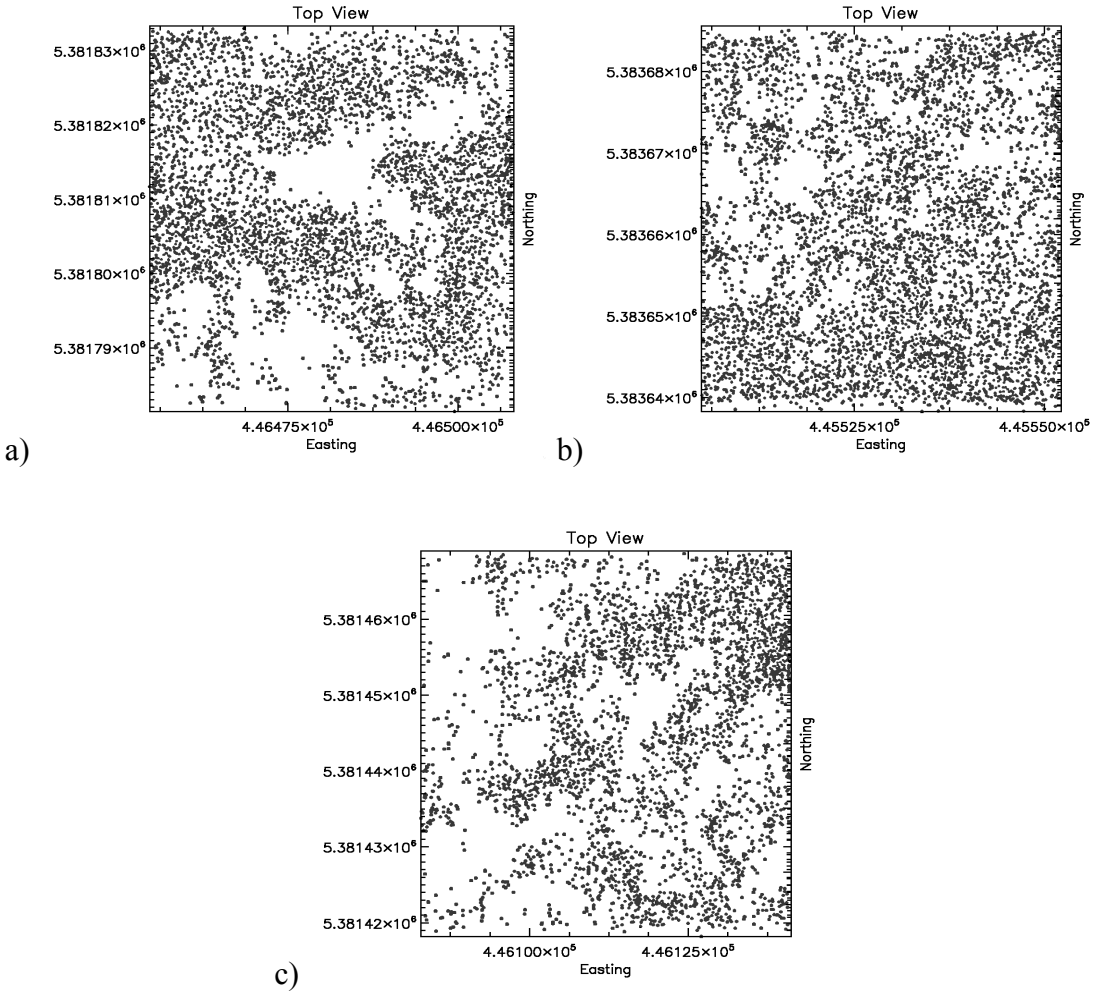


**Figure 38 - Plan-view of old-growth plots showing LiDAR points below TSCL.**

An increased amount of gaps in the old-growth plots was observed, revealing the vegetation underneath the dominant/co-dominant canopies. Also, the number of LiDAR points was higher close to the surface ground when compared to intermediate-growth plots (Figure 38) .

After analyzing the results for intermediate-growth and old-growth plots, it was clear that the algorithm was able to recognize where the "top of suppressed canopy level" boundary was located. What was also evident was an increased difficulty for the algorithm to identify this zone when the forest structure presented a more homogeneous vertical cover (like in: Plot 5 and Plot 7). Table 6 provides a summary of the results for all surveyed plots.

**Table 6 - Summary of number of partial-canopies identified. Column "Surveyed" represents the "intermediate" and "suppressed" trees surveyed in the field, while column "Identified" represents the number of trees identified by the algorithm based on the LiDAR points available below the TSCL threshold.**

| | Intermediate trees | |
|---|---|---|
| Plot# | Surveyed | Identified |
| 1 | 110 | 17 |
| 2 | 66 | 23 |
| 4 | 50 | 0 |
| 5 | 13 | 10 |
| 7 | 15 | 0 |
| 8 | 28 | 18 |

# Chapter 7: Discussion

The theory behind using remotely-sensed data and tree identification is well known and widely applied in the scientific research. As discussed in section 3.1, there were numerous papers reporting the use and possible applications of this idea. Many of the reported studies have dealt with relatively even-aged stands with more uniform vertical and horizontal structures. This study has attempted to adopt a methodology to apply to complex canopy structures.

## 7.1 – Tree crowns

The growth of a single tree was influenced by many different factors, such as: competition with other trees for light, nutrients, and water. This combination of factors created different levels of stress for individual trees, thus affecting how fast and how well the tree would develop. Having other trees nearby would also influence how individual canopies developed and grew. Even in a well-spaced tree plantation, canopies would interact, competing for space, affecting the shape of the individual crown and therefore, affecting the amount of leaf-area to receive energy from the sun. Wind was another factor that influenced the shape of a canopy, causing damages and sometimes causing the tree to fall down.

It is difficult to identify conifer trees that have uniform, conical canopy shape in a dense forested area. A tree with a single treetop, in dense areas, similar to this thesis' study area was also something difficult to be identified. In most cases, trees presented multiple treetops (Figure 39).

**Figure 39 - Uniform conifer tree shape on the left and tree with broken top and multiple tops on the right.**

## 7.2 – Treetop identification

Trees in young-growth plots were never taller than 20 m. Competition for light was never a problem observed in these plots because of the modest tree heights. Direct light was able to reach the entire tree canopy surface throughout the day. Because of the absence of competition for light, most of the tree canopies were commonly concentrated together. This concentration of trees added some difficulties for the algorithm to identify individual treetops, and usually a few trees close to each other were represented as one single tree.

Intermediate-growth plots did not present the same problems of young-growth plots. Throughout the years, competition for light and nutrients selected the most adapted trees able to survive, to grow, and to dominate the area. This caused trees with slower growth

rate to be suppressed underneath the dominant layer of vegetation. Interaction between tree canopies would still be present in the dominant layer, but now trees had a better well-defined canopy different from the young-growth plots trees. Examining the results of the identified treetops it was possible to observe that the algorithm performed well for intermediate-growth plots, having a high number of trees identified within plot boundaries. Intense interaction between canopies or broken tops was the most reasonable explanation for the treetops not identified by the algorithm. This caused confusion for the algorithm to recognize the beginning and end of tree crowns.

Old-growth plots had similar results compared to intermediate-growth plots, where canopies were well defined thus helping the algorithm in identifying treetops. Gaps were commonly seen in old-growth plots, helping in identifying treetops underneath the dominant layer of vegetation considerably. Confusion, when identifying a treetop, could have been introduced because of the large crown size of the old-growth trees. Large crowns had a higher probability of presenting multiple treetops, broken tops, and large gaps, creating extra difficulties for the algorithm to identify the real treetop.

### 7.3 – Matching surveyed and identified treetops

The only method to assess the performance of the algorithm in identifying trees was to match surveyed tree coordinates acquired using a LASER rangefinder instrument mounted on a tripod in the field, with coordinates for the trees identified by the algorithm. This method had its limitations because the surveyed coordinates represented the base of the tree in the study area, whereas the coordinates obtained with the algorithm

represented the top of the canopy. It would not be a problem if the trees were perfectly straight, and had a perfect conical-shaped canopy. However, many trees in the study area did not fulfill this requirement. Depending on how tall the tree was, the coordinates for the treetop and the coordinate surveyed at ground level were a few metres apart. The algorithm for matching these coordinates tried to take this problem into account by adding a buffer zone to locate and match both coordinate pairs. This buffer zone represented a circular search area from the identified treetop with the same maximum radius used to identify the dominant and co-dominant trees for each plot.

The GPS signal strength dropped drastically below dense canopies, so that an accurate absolute positioning of the individual stems was not possible. Another problem that could have led to a lower percentage of identified/matched trees was the classification used for determining tree dominance. Different field surveyors were used to classify the trees, which might have caused misclassification of dominant trees.

## 7.4 – Crown delineation

### 7.4.1 – Young-growth plots

Young-growth areas presented high stem density and dense understory vegetation. To reduce the amount of time surveying the plots located in these young-growth areas, and to provide better quality of collected data it was decided to decrease the plots size from 40 x 40 m to 20 x 20 m. For young plots, the delineated crowns presented multiple crown shapes most of the time. The classic conical-shape was rarely seen in these plots because

of the small tree heights and density of trees. The young age of these trees and the high interaction with surrounding canopies did not provide well-defined canopies.

### 7.4.2 – Intermediate-growth plots

Plot 1 was the first plot to be surveyed in the field. It was an interesting plot because of the homogenous tree heights that could be observed once inside. Dominant trees reached maximum heights of around 30 m and patches of highly suppressed trees never reached more than 1.5 m. Tree canopies were constantly interacting and competing for space and light in this dense stand plot. It was possible to observe this interaction on figure 27 (d-f), LiDAR background and delineated crowns, where there was no visible distinction of beginning and end of crown. Even so, the algorithm was able to delineate the crowns around the treetops previously identified.

Similarly to plot 1, plot 4 presented high density of trees and homogeneous tree heights within the plot. The difference was the reduced amount of vegetation underneath the dominant layer of vegetation. Examining the LiDAR image (Figure 27e) it was possible to observe the constant interaction, similar to plot 1, of canopies throughout the plot, and fewer gaps.

Plot 7, the last intermediate-growth plot surveyed, was located on the west side of the valley, where the terrain presented a slope close to 35°. The trees still presented homogeneous heights throughout. The difference between this plot and the previous ones was the increased presence of highly suppressed trees.

Even in plots with high density of trees and constant interaction of canopies, the algorithm performed well when delineating tree crowns. The average difference between surveyed and delineated crown size was 0.7 m.

### 7.4.3 – Old-growth plots

Plot 2 represented a different scenario for trees in Rithet Valley. This plot was located right beside the main creek of the valley and presented the tallest trees of all the plots surveyed. As observed in figure 27g, the plot presented different layers of vegetation. Bright pixels represented dominant trees and darker pixels represent trees underneath the dominant layer. The algorithm delineated the dominant crowns as well the visible trees underneath this layer.

Plot 5 was located close to the top of the Rithet Creek valley. The area presented no significant slope but a few small hills along the plot. The concentration of salal in this plot was intense, reaching heights greater than 1 m in certain areas. Interaction of tree canopies was more intense in this plot than plot 2 among dominant/co-dominant trees. Even so, the algorithm was able to delineate tree crowns of the dominant layer, as well as crowns of lower trees visible through gaps.

Plot 8 presented a higher number of old-growth trees compared to plot 2 and plot 5. Even presenting an elevated amount of gap fraction, intermediate and suppressed trees were

located most of the time underneath the dominant layer of vegetation, not visible through gaps. The algorithm also presented good results for this plot, where most of the trees were properly delineated.

The method used to measure the crown-width in the field consisted in using a tape to measure the crown from the ground, extending it, and looking up until the end of the crown was reached. Error could be introduced in using this method once there were different people acquiring the data. Also, the perception of the end of a crown might differ among surveyors.

### 7.5 – Partial crowns identification

As described in section 5.4, the method for the partial crowns identification focused in automatically identifying the vegetation layer that holds potential fuel ladder in a particular study plot. This identification was possible by observing the difference in density between vertical forest profiles. Identifying such change in the field would bring an enormous amount of biased data since it was a very subjective measurement, especially if not collected by the same surveyor every time. The top of suppressed canopy level (TSCL) was affected by many factors, such as: stem density and wind. Stem density related to how many trees were distributed in an area. Dense plots would have high competition for natural resources, where light represented the most important variable, describing the tree location/position and canopy orientation. Also, fast growing tree canopies would cover trees with slower growth rate. The number of trees among other

trees would also influence how branches spread, and when strong winds strike the area, the possibility of broken branches increased.

The method used for this module had a lower accuracy when the different vegetation layers had a more homogeneous density, being almost impossible to visually distinguish layers. This problem may be solved with newer LiDAR systems, where the density of pulse returns per square metre is increased and higher frequencies are used. Higher number of return points would be able to penetrate more efficiently through every layer, increasing the detail of the forest structure, especially for understory vegetation.

Intermediate-growth and old-growth stands were used to test the capabilities of this module, because older and taller trees present larger gaps. Usually, taller trees were subjected to strong winds that break branches and treetops. Larger and more numerous gaps made it possible for LiDAR pulses to reach deeper into the canopy. In other words, the density of points found in between the canopy and ground surface increased and enhanced the chance of identifying LiDAR points that represented partial canopies of trees that grew underneath dominant ones.

For old-growth plots, the best way of testing the algorithm was to identify trees classified as intermediate-growth trees within this plot. Intermediate-growth trees were classified as those that had their canopy covered by one or more taller trees (dominant or co-dominant trees). These intermediate-growth trees were typically half the size of dominant trees. Therefore, these trees had the potential to be identified by the algorithm, as they had enough height to not be confused with any other object close to the ground such as bushes, rocks or fallen trees.

# Chapter 8: Conclusion

## 8.1 – Conclusions

In general, the algorithms developed here performed well, providing output that were envisioned at the early stages of development of the computer code. It was shown that it is possible to identify treetops and delineate their crowns using raw data, avoiding gridding of the LiDAR data and applying methods to create a smooth dataset. On average, intermediate and old-growth plots had more than 80% of the trees successfully identified and matched with the field data. The percentage for young-growth plots was lower, with an average greater than 70%. This was probably due to the LiDAR posting density. Small young canopies and large concentration of trees created a scenario where the posting density of the LiDAR system was not able to discriminate where one crown ended and another one started. This not only created difficulties in the identification of all the treetops in the study area, but also in the delineation of each tree crown. For young-growth plots the averaged difference between field surveyed crown data and delineated by the computer algorithm was 0.6 m. Old-growth plots presented the best delineated crowns with an averaged difference of 0.34 m.

Further tuning of the individual treetop identification and crown delineation algorithms is still necessary. A disadvantage of using raw data was the increase of time spent in the identification and delineation of tree canopies. The author recognizes that there is still a long way to go tuning the algorithm, and making data processing faster.

The partial canopies identification module, as previously stated, is still a preliminary study to explore the issues encountered in the field data collection and the development of the algorithm. Only a few trees were identified using this method , thus showing that this might not be the most appropriate approach to be used in densely-forested areas.

Furthermore, the field data collection process needs improvement, particularly in collecting data with the highest accuracy. Special attention must be given to collecting tree locations and assessing study plot vertices. A higher accuracy GPS is required to gather strong signals underneath the thick canopies. Collecting accurate tree locations will provide a better dataset to match against the identified treetops by the computer algorithm. Also, each instrument should be managed by only one person during the entire survey. Biasing of the data will be minimized if this requirement is followed.

## 8.2 – Future work

Further studies with the algorithm will also focus in heterogeneous areas, where Douglas-fir is not the dominant tree species. Also, the computer algorithms developed here will be tested with new datasets acquired from new LiDAR systems. These new datasets are comprised of a large number of points per square metre, thus presenting a new challenge for the algorithms. A more accurate crown delineation will be expected from these new datasets.

# Bibliography

Ackermann, F. (1999) Airborne laser scanning-present status and future expectations. *ISPRS Journal of Photogrammetry and Remote Sensing* 54(2): 64-67.

Andersen, H., S. Reutebuch, & G. Schreuder (2001) Automated individual tree measurement through morphological analysis of a LIDAR-based canopy surface model. In: *Proceedings of the First International Precision Forestry Symposium*, Seattle, WA, USA.

Axelsson, P. (1999) Processing of laser scanner data-algorithms and applications. *ISPRS Journal of Photogrammetry & Remote Sensing* 54: 138-147.

BCStats, url: http://www.bcstats.gov.bc.ca/, accessed in September 15, 2008.

Bortolot, Z. J. & Wynne, R. H. (2005) Estimating forest biomass using small footprint LiDAR data: An individual tree-based approach that incorporates training data. *ISPRS Journal of Photogrammetry & Remote Sensing* 59(6): 342-360.

Brandtberg, T. & Walter, F. (1998) Automated delineation of individual tree crowns in high spatial resolution aerial images by multiple-scale analysis. *Machine Vision and Applications* 11(2): 64-73.

Chen, Q., Baldocchi , D. D., & Gong, P. (2006) Isolating individual trees in a savanna woodland using small footprint LIDAR data. *Photogrammetric Engineering Remote & Remote Sensing* 72(8): 923-932.

Clark, M. L., Clark, D. B. & Roberts, D. A. (2004) Small-footprint lidar estimation of sub-canopy elevation and tree height in a tropical rain forest landscape. *Remote Sensing of Environment* 91: 68-89.

Cobby, D. M., Mason, D.C. & Davenport, I.J. (2001) Image processing of airborne scanning laser altimetry data for improved river flood modeling. *ISPRS Journal of Photogrammetry & Remote Sensing* 56: 121-138.

Culvenor, D. S. (2002) TIDA: An algorithm for the delineation of tree crowns in high spatial resolution digital imagery of Australian native forest, *Ph.D. dissertation*, University of Melbourne, Melbourne, Australia.

Diedershagen, O., Koch, B. & Weinacker, H. (2003) Automatic estimation of forest inventory parameters based on lidar, multi-spectral and fogis data. In: *Proceedings Optical 3-D Measurement Techniques VI*: 259-269.

Dralle, K. & Rudemo, M. (1996) Stem number estimation by kernel smoothing in aerial photos. *Canadian Journal of Forest Research* 26: 1228–1236.

Dralle, K. & Rudemo, M. (1997) Automatic estimation of individual tree positions from aerial photos. *Canadian Journal of Forest Research* 27:1728–1736.

Gomez, M., Serrano, A. & Casalprim, D. (2005) Generation of a DTM based on Lidar Data for the definition of Hydraulic Moldels. In: *XII International Cartographic Conference. Spain.*

Gougeon, F. A. (1999) Automatic individual tree crown delineation using a valley-following algorithm and rule-based system. In: *Proceedings International Forum on Automated Interpretation of High Spatial Resolution Digital Imagery for Forestry*, Victoria, B.C.; Canada 11:23

Gougeon, F. A. & Leckie, D. G. (2006) The individual tree crown approach applied to Ikonos images of a coniferous plantation area. *Photogrammetric Engineering Remote & Remote Sensing* 72:1287–1297

Hopkinson, C., Chasmer, L., Young-Pow, C. & Treitz, P. (2004) Assessing forest metrics with a ground-based scanning lidar. *Journal of Forest Research* 34: 573-583.

Katoh, M., Gougeon, F. A. & Leckie, D. G. (2009) Application of high resolution airborne data using individual tree crowns in Japanese conifer plantations. *Journal of Forest Research* 14: 10-19.

Koch B., Heyder U. & Weinacker, H. (2006) Detection of Individual Tree Crowns in Airborne LiDAR Data. *Photogrammetric Engineering Remote & Remote Sensing* 72: 357-363.

Kraus, K. & Pfeifer, N. (1998) Determination of terrain models in wooded areas with airborne laser scanner data. *ISPRS Journal of Photogrammetry & Remote Sensing* 53: 193-203.

Kwak, D. A., Lee, W. K., Lee, J. H., Biging, G. S. & Gong. P. (2007). Detection of individual trees and estimation of tree height using LiDAR data. *Journal of Forest Research* 12: 425-434.

Larsen, M. & Rudemo, M. (1997) Using ray-traced templates to find individual trees in aerial photos. In: *Proceedings of the 10th Scandinavian Conference on Image Analysis*, Lappeenranta, vol. 2, pp. 1007–1014

Lefsky M. A. ,Harding D., Cohen W. B. & Parker G. G. (1999a). Surface lidar remote sensing of the basal area and biomass in deciduous forests of eastern Maryland, USA. *Remote Sensing of Environment* 67: 83–98.

Lefsky M. A., Cohen W. B., Acker S. A., Spies T. A., Parker G. G. & Harding D. (1999b) Lidar remote sensing of biophysical properties and canopy structure of forest of Douglas-fir and western hemlock. *Remote Sensing of Environment* 70: 339–361.

Lefsky, M. A., Cohen, W. B., Parker, G. G., & Harding, D. J. (2002) Lidar remote sensing for ecosystem studies. *Bioscience* 52: 19– 30.

Lim, K., Treitz, P., Groot, A. & St-Onge, B. (2001) Estimation of Individual Tree Heights Using LiDAR Remote Sensing. In: *Proceedings of the 23rd Canadian Journal of Forest Research* 1: 243-250.

Lim, K., Treitz, P., Wulder, M., St-Onge, B. & Flood, M. LiDAR (2003) Remote sensing of forest structure, *Progress in Physical Geography* 27: 88–106.

Lohr, U (2003) Toposys, Precise Lidar DEM and True Ortho Photos. In: *Photogrammetric Week 03*.

Maltamo, M., Tokola, T. & Lehikoinen, M. (2003) Estimating stand characteristics by combining single tree pattern recognition of digital video imagery and a theoretical diameter distribution model. *Forest Science* 49: 98-109.

Matsugami, H., Shimizu, Y. & Omasa, K. (2005) Detection of tree apexes from helicopter-borne scanning lidar data using local maximum filtering. *Phyton-Annales Rei Botanicae* 45(4): 501-504.

Næsset, E. (1997a) Determination of mean tree height of forest stands using airborne laser scanner data. *ISPRS Journal of Photogrammetry and Remote Sensing* 52: 49–56.

Næsset, E. (1997b) Estimating timber volume of forest stands using airborne laser scanner data. *Remote Sensing of Environment* 61: 246– 253.

Næsset, E., & Bjerknes, K. O. (2001) Estimating tree heights and number of stems in young forest stands using airborne laser scanner data. *Remote Sensing of Environment* 78: 328-340.

Næsset, E. & Økland, T. (2001) Estimating tree height and tree crown properties using airborne scanning laser in a boreal nature reserve. *Remote Sensing of Environment* 79: 105-115.

Næsset, E. (2002) Predicting forest stand characteristics with airborne scanning laser using a practical two-stage procedure and field data. *Remote Sensing of Environment* 80: 88-99.

Natural Resources Canada, 2007. Canada's Forest Statistical Data. Url: http://canadaforests.nrcan.gc.ca/statsprofile/forest/ca, accessed in September 15, 2008

Nayegandhi, A., Brock, J. C., Wright, C. W. & O'Connel, M. J. (2006) Evaluating a small footprint, waveform resolving Lidar over coastal vegetation communities.. *Photogrammetric Engineering & Remote Sensing* 72: 1407-1415.

Niemann, K. O., Adams, S., & Hay, G. (1999) Automated tree crown identification using digital orthophoto mosaics. In: *Proceedings of the International Forum on*

*Automated Interpretation of High Spatial Resolution Digital Imagery for Forestry*, Victoria, B.C., Canada: 105–108.

Persson, Å., Holmgren, J., & Söderman, U. (2002) Detecting and measuring individual trees using an airborne laser scanner. *Photogrammetric Engineering & Remote Sensing* 68: 925–932.

Popescu, S. C., Wynne, R. H. & Nelson, R. F. (2002) Estimating plot-level tree heights with lidar: local filtering with a canopy-height based variable window size. *Computers and Electronics in Agriculture*, 37(1-3): 71-95.

Riano, D., Meier, E., Allgower, B., Chuvieco, E. & Ustin, S.L. (2003) Modeling airborne laser scanning data for the spatial generation of critical forest parameters in fire behavior modeling. *Remote Sensing of Environment* 86: 177-186.

Takahashi, T., Yamamoto, K., Miyachi, Y., Senda, Y. & Tsuzuku, M. (2006) The penetration rate of laser pulses transmitted from a small-footprint airborne LiDAR: a case study in closed canopy, middle-aged pure sugi (Cryptomeria japonica D. Don) and hinoki cypress (Chamaecyparis obtuse Sieb. Et Zucc.) stands in Japan. *Journal of Forest Research* 11: 117-123.

Uuttera, J., A. Haara, T. Tokola, & M. Maltamo (1998) Determination of the spatial distribution of trees from digital aerial photographs. *Forest Ecology and Management*, 110:275–282.

Vosselman, G. & Maas, H. G. (2001) Adjustment and filtering of raw Laser altimetry data. *OEEPE Official Publication* 40:62–72.

Wehr, A. & Lohr, U. (1999). Airborne laser scanning—an introduction and overview. *Journal of Photogrammetry & Remote Sensing* 54: 68-82.

Wolf, B. M & Heipke, C., 2007. Automatic extraction and delineation of single trees from remote sensing data. *Machine Vision and Applications* 18: 317-330.

Wu, L., Zhang, Y., Gao, Y., ZHANG (1) & Zhang, Y. Tree crown detection and delineation in high resolution RS image : A texture approach discussion. In: *IGARSS 2004* 7:CVIII-4916

Wulder, M., Niemann, K. O. & Goodenough, D.G. 2000. Local maximum filtering for the extraction of tree locations and basal area from high spatial resolution imagery. *Remote Sensing of Environment* 73: 103–114.

Wulder, M. A., White, J. C., Niemann, K. O. & Nelson, T. (2004) Comparison of airborne and satellite high spatial resolution data for the identification of individual trees with local maxima filtering. *International Journal of Remote Sensing*, 25(11): 2225-2232.

Yu, X., Hyyppa, J., Kaartinen, H. & Maltamo, M. (2004). Automatic detection of harvested trees and determination of forest growth using airborne laser scanning. *Remote Sensing of Environment*, 90: 451-462.

Zhang, K. et al. (2003). A Progressive Morphological Filter for Removing Nonground Measurements From Airborne LIDAR Data. In: *Transactions on Geoscience and Remote Sensing*, 41(4): 872-882.

# Appendix A – Study plots with tree locations

Convex hull is the boundary of the minimal convex set containing all the trees surveyed for each plot. Each tree is represented by a diamond symbol.

a) Young-growth plots

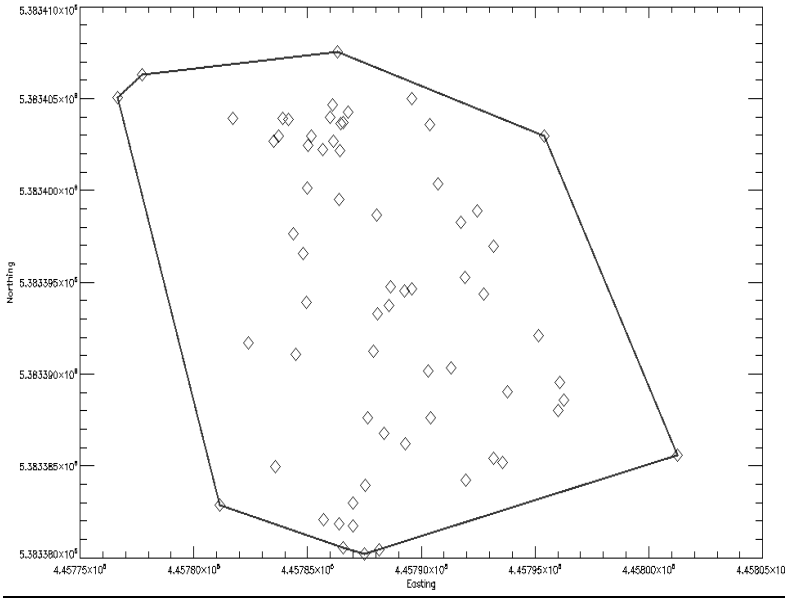


Figure 1 – Plan view of plot 3 with individual surveyed tree locations (diamond shapes) and convex hull (line)

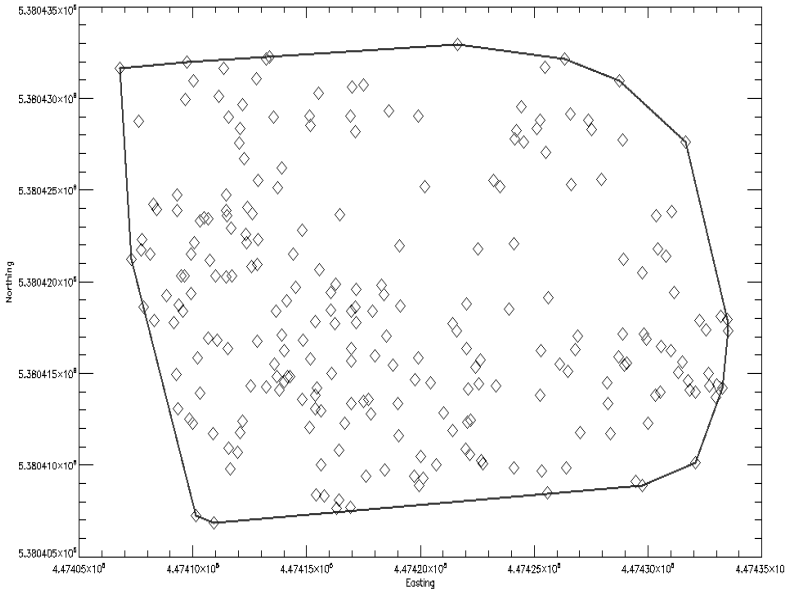


Figure 2 – Plan view of plot 6 with individual surveyed tree locations (diamond shapes) and convex hull (line)

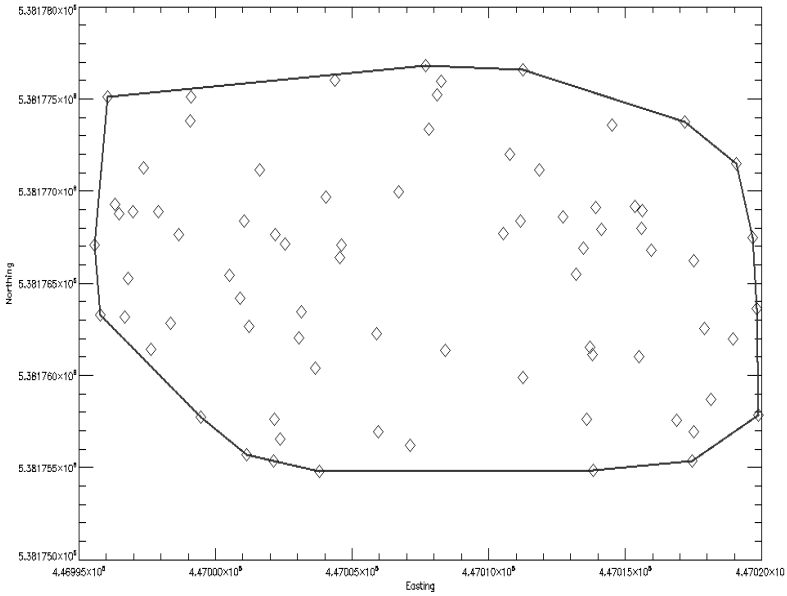


Figure 3 – Plan view of plot 9 with individual surveyed tree locations (diamond shapes) and convex hull (line)

b) Intermediate-growth plots

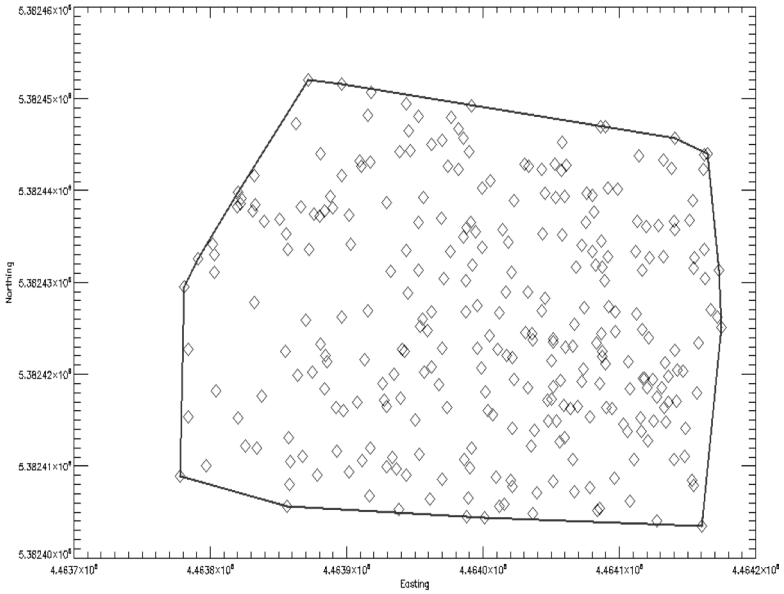


Figure 4 – Plan view of plot 1 with individual surveyed tree locations (diamond shapes) and convex hull (line)

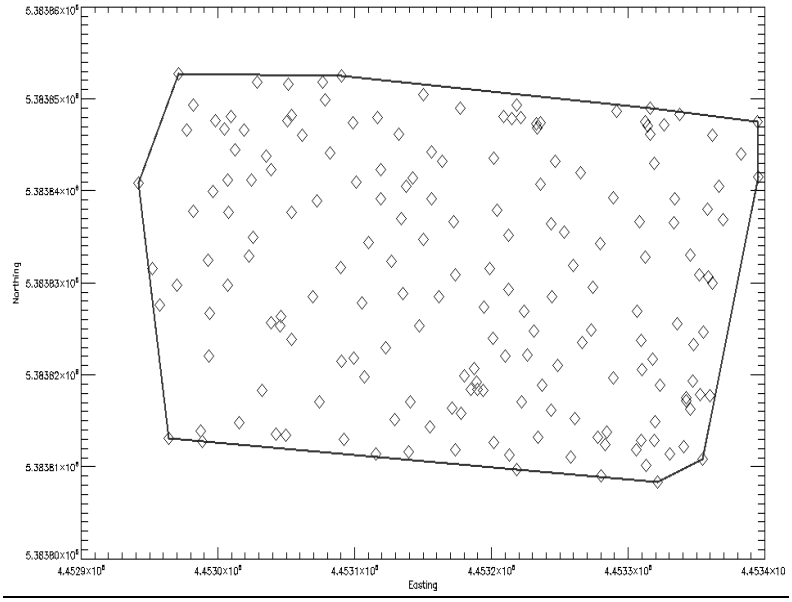


Figure 5 – Plan view of plot 4 with individual surveyed tree locations (diamond shapes) and convex hull (line)

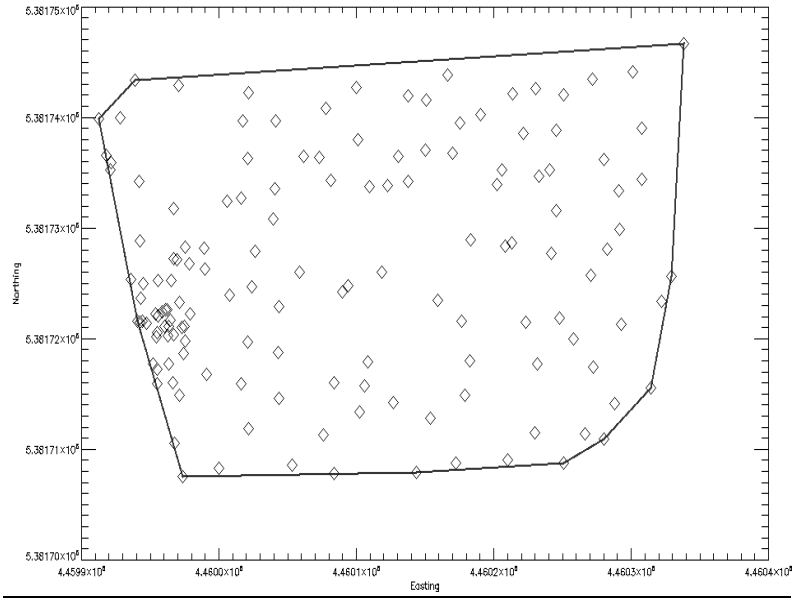


Figure 6 – Plan view of plot 7 with individual surveyed tree locations (diamond shapes) and convex hull (line)

c) Old-growth plots

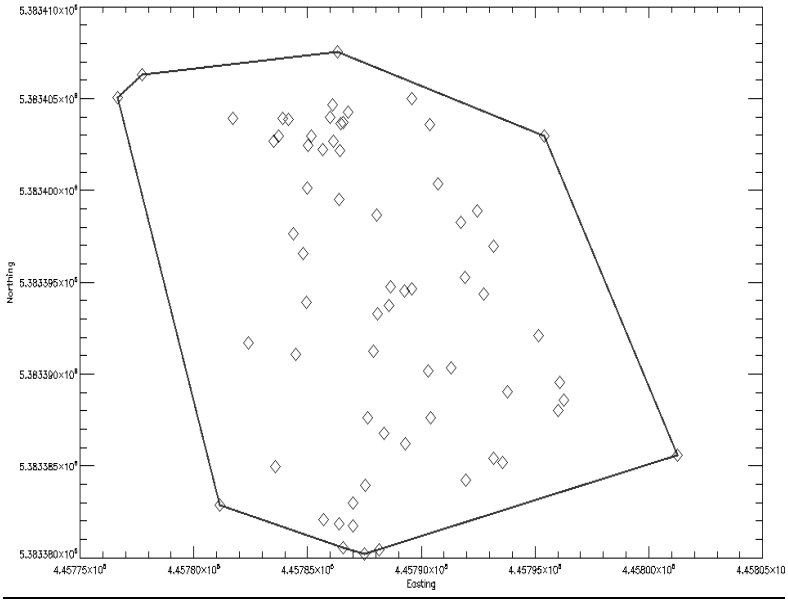


Figure 7 – Plan view of plot 2 with individual surveyed tree locations (diamond shapes) and convex hull (line)

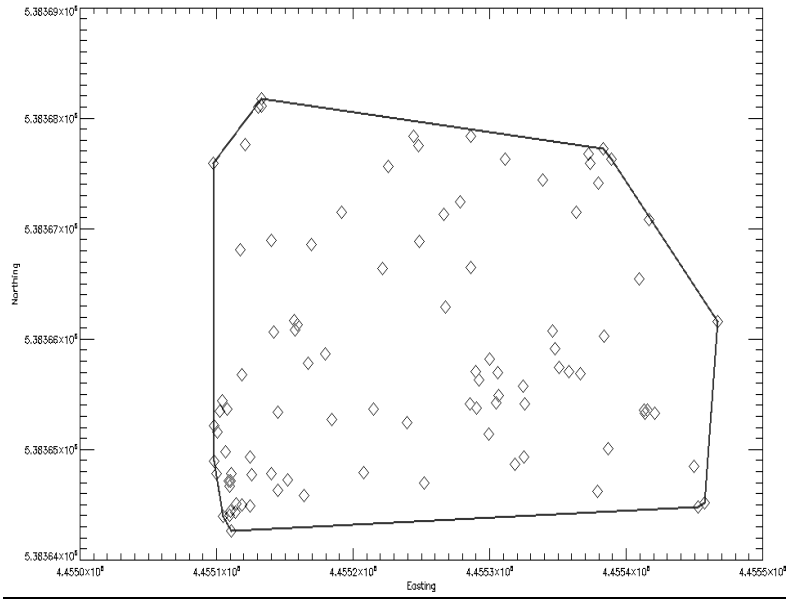


Figure 8 – Plan view of plot 5 with individual surveyed tree locations (diamond shapes) and convex hull (line)

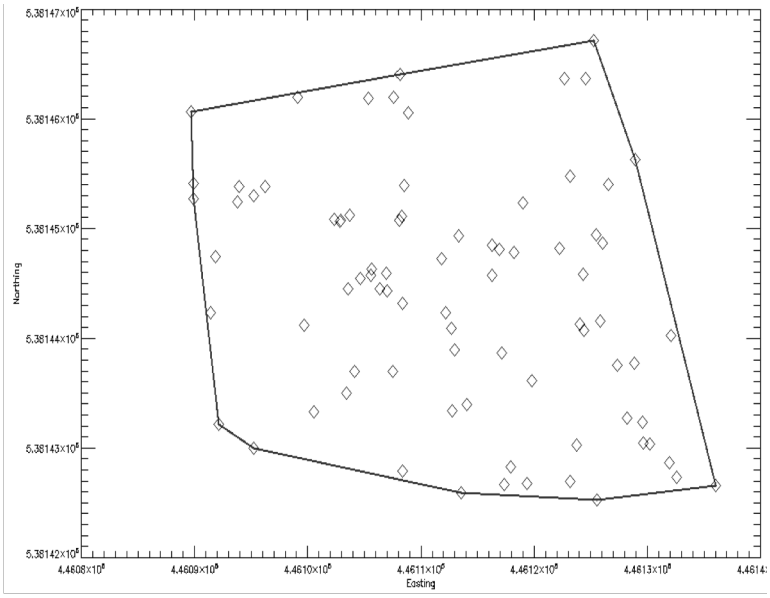


Figure 9 – Plan view of plot 8 with individual surveyed tree locations (diamond shapes) and convex hull (line)